PHYSICAL REVIEW D **93,** 094515 (2016)

Novel quark smearing for hadrons with high momenta in lattice QCD

Gunnar S. Bali,[1,2,*] Bernhard Lang,[1,†] Bernhard U. Musch,[1,‡] and Andreas Schäfer[1]
(RQCD Collaboration)

[1]*Institut für Theoretische Physik, Universität Regensburg, 93040 Regensburg, Germany*
[2]*Department of Theoretical Physics, Tata Institute of Fundamental Research, Homi Bhabha Road, Mumbai 400005, India*

(Received 23 February 2016; published 27 May 2016)

Hadrons in lattice QCD are usually created employing smeared interpolators. We introduce a new quark smearing that allows us to maintain small statistical errors and good overlaps of hadronic wave functions with the respective ground states, also at high spatial momenta. The method is successfully tested for the pion and the nucleon at a pion mass $m_\pi \approx 295$ MeV and momenta as high as 2.8 GeV. We compare the results obtained to dispersion relations and suggest further optimizations.

DOI: 10.1103/PhysRevD.93.094515

I. INTRODUCTION

Lattice QCD simulations predict an ever increasing number of observables that are relevant to particle and hadron physics phenomenology. These results are usually extracted from expectation values of n-point functions at large Euclidean time separations. Due to the decay of these functions with time, statistical noise over signal ratios increase exponentially as time separations are taken large (with the notable exception of pseudoscalar mesons at zero momentum). Fortunately, there exists some freedom in the construction of interpolators for the creation of mesonic and baryonic states. Employing interpolators that resemble the spatial structure of the ground state wave function enables asymptotic results to be extracted at time separations where the signal over noise ratio is still large.

Many applications nowadays demand hadrons that carry momentum. For instance, pushing the calculation of semileptonic decay form factors for $B \to \pi \ell \bar{\nu}_\ell$ or $\Lambda_b \to p \ell \bar{\nu}_\ell$ [1] toward small virtualities requires spatial momenta of the size of the mass difference between the B meson and the pion or between the Λ_b baryon and the proton, respectively. Another important type of application are parton distribution functions (PDFs) and their generalizations, in particular transverse momentum dependent parton distribution functions (TMDs), or Wigner distributions as a whole. Also these quantities are extracted from matrix elements of the type $\langle H(\boldsymbol{p}')|\mathcal{O}|H(\boldsymbol{p})\rangle$, where $H(\boldsymbol{p})$ is a hadron state with momentum $\boldsymbol{p}$. The operator $\mathcal{O}$ cannot have an extent in Minkowski-time on the Euclidean lattice. Therefore, in order to extrapolate to light front kinematics for an inherently nonlocal operator, one has to work in a frame of reference where hadrons carry high spatial momenta $\boldsymbol{p}, \boldsymbol{p}'$. This fact has been known for quite some time in the context of lattice calculations of TMDs [2–4] and is illustrated very clearly in recent work on these distributions in the pion [5]. For the same reason fast hadrons on the lattice are highly desirable in a new scheme proposed to relate quasi parton distributions to light front distributions in a controlled manner [6,7]. First lattice computations in this direction have started [8,9]. Earlier suggestions to compute quasi distribution amplitudes in position space [10–12] equally require pions or nucleons at high momenta. Unfortunately, up to now no satisfactory techniques for hadrons carrying high momenta existed to suppress excited state contributions.

To be more specific, a two-point function is given as

$$C_H(t) = \langle H(t) H^\dagger(0)\rangle = \sum_{j>0} \frac{|\langle j|\hat{H}^\dagger|0\rangle|^2}{2E_{H,j}} e^{-E_{H,j}t}, \qquad (1)$$

where $E_{H,j}$ denotes the jth energy level within the tower of states created by the interpolator $H^\dagger$. Obviously, the contribution of the jth excited state is suppressed relative to the ground state not only by $\exp[-(E_{H,j} - E_{H,1})t]$ but also by the ratio $|\langle j|\hat{H}^\dagger|0\rangle|^2/|\langle 1|\hat{H}^\dagger|0\rangle|^2$: increasing the ground state overlap factor $|\langle 1|\hat{H}^\dagger|0\rangle|$, relative to $|\langle j|\hat{H}^\dagger|0\rangle|$ for $j > 1$, results in an additional suppression of excitations.

Reducing excited state overlaps by employing extended interpolators was first pursued in computations of the glueball spectrum. In this case the gauge links within the corresponding interpolators can be iteratively "APE smeared" [13], "fuzzed" [14] or "HYP smeared" [15], to better approximate the (smooth) ground state wave function, see also Ref. [16]. This gauge link smearing was subsequently generalized to iterative smearing of quark fields within interpolators that create mesonic and baryonic states, in particular gauge covariant Wuppertal (i.e. Gauß)

*gunnar.bali@ur.de
†bernhard.lang@physik.uni-regensburg.de
‡bmusch@jlab.org

smearing [17–19], hydrogen-like smearing [19] as well as Jacobi smearing [20,21]. Additionally, in Refs. [18,19,22] APE smearing was employed for the spatial gauge transporters within the quark smearing while in Ref. [22] linear combinations of different levels of Wuppertal smearing were utilized.

Since Gaussian smearing functions may not be optimal for creating, e.g., p-waves, even when adding derivatives to the interpolator, iterative smearing was later-on combined with displaced quark sources (fuzzing) in Ref. [23], a generalization of which was suggested in Ref. [24]. Finally, in Ref. [25] "free form smearing", folding Gaussian smearing with an arbitrary function in a gauge covariant way, was invented. Preceding and in parallel to gauge covariant iterative smearing functions, gauge fixed sources have been utilized: wall sources for zero [26] and nonzero momentum [27], box [28] sources, Gaussian "shell sources" [29] and sources with nodes [30]. These gauge fixed methods and free form smearing share the disadvantage that smearing the sink requires all quark positions to be summed over individually, turning this prohibitively expensive. Having identical source and sink interpolators, however, is very desirable as only this guarantees the positivity of the coefficients of the spectral decomposition Eq. (1) and thus the convexity of two-point functions. For completeness, we also mention the "distillation" (or Laplacian-Heaviside) method of Ref. [31] since this is closely related to gauge covariant smearing.

Large momenta increase the energy of the state and result in faster decaying two- and three-point functions and, therefore, in inferior noise to signal ratios. Moreover, as we shall see, excited state suppression becomes far less effective when using conventional quark smearing methods. Some attempts have been made [32,33] to introduce an anisotropy into Wuppertal smearing [17,18], aiming at Lorentz contracting the interpolating wave function according to the boost factor $1/\gamma = m/E(\boldsymbol{p})$, along the direction of the spatial momentum $\boldsymbol{p}$. However, this did not result in the ground state enhancement that one would have hoped for. Here we will argue and demonstrate that to achieve satisfactory results at high momenta, additional phase factors need to be incorporated into quark smearing functions.

This article is organized as follows. First, in Sec. II, we discuss the basic idea behind the new class of smearing functions that we introduce. Then, in Sec. III we are more specific, modifying Wuppertal smearing as a generic example and suggest further improvements. In Sec. IV we discuss our simulation parameters and expectations for the nucleon and pion energies. After the stage is set, in Sec. V we investigate the feasibility of the method in a realistic numerical study, optimize the smearing parameters and pursue a comparison between the new and the conventional method. Finally, we study the pion and nucleon dispersion relations, before we conclude.

II. MOMENTUM SMEARING: THE BASIC IDEA

As discussed above, quark smearing within hadronic sources or sinks is essential in lattice simulations to increase the overlap with the desired physical state, reflecting the fact that hadrons are extended objects, rather than pointlike. A smearing operator F is diagonal in time, trivial in spin and acts on the position and color indices of quark fields:

$$(Fq)_{\boldsymbol{x}} = \sum_{\boldsymbol{y}\in(a\mathbb{Z})^d} f_{\boldsymbol{x}-\boldsymbol{y}} G_{\boldsymbol{x}\boldsymbol{y}} q_{\boldsymbol{y}}, \tag{2}$$

where f is a scalar function, G is a gauge covariant transporter, which in the free case will be a unit matrix in color and position space, and d is the number of spatial dimensions, usually $d = 3$. Note that the field $q_{\boldsymbol{x}}$ is usually periodic in $\boldsymbol{x}$ on the lattice, whereas $f_{\boldsymbol{x}-\boldsymbol{y}}$ need not be periodic in $\boldsymbol{x}-\boldsymbol{y}$. In the free case, the convolution Eq. (2) becomes a product in Fourier space

$$\sum_{\boldsymbol{x}\in(a\mathbb{Z})^d} e^{i\boldsymbol{p}\cdot\boldsymbol{x}} (Fq)_{\boldsymbol{x}} = \tilde{f}(\boldsymbol{p})\tilde{q}_{\boldsymbol{p}}. \tag{3}$$

For the special case of a Gaussian,

$$f_{\boldsymbol{x}-\boldsymbol{y}} = f_{\boldsymbol{0}} \exp\left(-\frac{|\boldsymbol{x}-\boldsymbol{y}|^2}{2\sigma^2}\right), \tag{4}$$

the Fourier transformed smearing kernel again is a Gaussian:

$$\tilde{f}(\boldsymbol{p}) \equiv \sum_{z\in(a\mathbb{Z})^d} e^{i\boldsymbol{p}\cdot z} f_z = \tilde{f}(\boldsymbol{0}) \exp\left(-\frac{\sigma^2\boldsymbol{p}^2}{2}\right). \tag{5}$$

Thus, the smeared quark operator has maximal overlap with a quark at rest, $\boldsymbol{p} = \boldsymbol{0}$. Nonzero velocities are suppressed in accordance with the above Gaussian momentum distribution. Clearly, for hadrons carrying significant spatial momenta, such a smearing may be counterproductive.

Having identified the problem, it is easy to modify the smearing to perform well for moving hadrons. We aim at a momentum distribution of quarks centred around a finite momentum $\boldsymbol{k}$, so we need to shift the smearing kernel in momentum space:

$$\tilde{f}(\boldsymbol{p}) \mapsto \tilde{f}(\boldsymbol{p}-\boldsymbol{k}), \tag{6}$$

as illustrated in Fig. 1. This translates to the replacement in position space

$$f_z \mapsto e^{i\boldsymbol{k}\cdot z} f_z. \tag{7}$$

Our modified smearing operator $F_{(\boldsymbol{k})}$, where $F_{(\boldsymbol{0})} = F$, can thus be formally expressed as

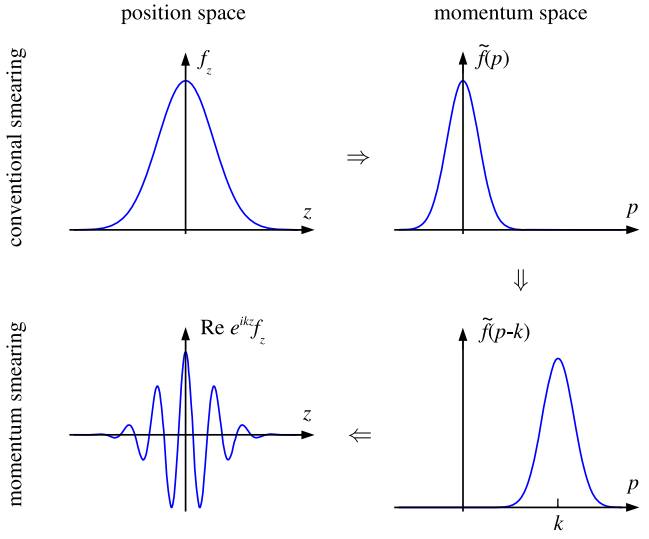

FIG. 1. Conventional smearing versus momentum smearing for the example of a Gaussian wave function in $d = 1$ spatial dimensions. The momentum k shifts the center of the distribution in momentum space, resulting in an oscillatory behavior in position space.

$$(F_{(\boldsymbol{k})}q)_{\boldsymbol{x}} = \sum_{\boldsymbol{y}\in(a\mathbb{Z})^d} F_{(\boldsymbol{k})\boldsymbol{xy}}q_{\boldsymbol{y}} = \sum_{\boldsymbol{y}\in(a\mathbb{Z})^d} e^{-i\boldsymbol{k}\cdot(\boldsymbol{x}-\boldsymbol{y})}f_{\boldsymbol{x}-\boldsymbol{y}}G_{\boldsymbol{xy}}q_{\boldsymbol{y}}. \tag{8}$$

The only new ingredient is the additional phase factor $\exp[-i\boldsymbol{k}\cdot(\boldsymbol{x}-\boldsymbol{y})]$. Note that the quark momentum shift $\boldsymbol{k}$ need *not* be a lattice momentum, i.e. it is not restricted to discrete values $\boldsymbol{k} \in (2\pi/L)\mathbb{Z}^d$. The smearing kernel f and the gauge dependent factor G can be taken over from any existing smearing method. For an iterative smearing method, the extra phase factor can easily be integrated into the elementary smearing step. Below we demonstrate this for the example of Wuppertal smearing. In principle, there could be additional effects like a Lorentz contraction of the wave function. This was studied, e.g., in Refs. [32,33], and we will also address this possibility.

The new, modified smearing operator $F_{(\boldsymbol{k})}$ of Eq. (8) inherits important properties from the smearing operator $F_{(\boldsymbol{0})}$ it is based on. If the unmodified smearing operator is self-adjoint, then so is the modified smearing operator $F_{(\boldsymbol{k})}$, because from $f_{\boldsymbol{x}-\boldsymbol{y}} = f^*_{\boldsymbol{y}-\boldsymbol{x}}$ and $G_{\boldsymbol{xy}} = G^\dagger_{\boldsymbol{yx}}$ it follows that $F_{(\boldsymbol{k})\boldsymbol{xy}} = F^\dagger_{(\boldsymbol{k})\boldsymbol{yx}}$. The underlying smearing operator $F_{(\boldsymbol{0})}$ should transform according to an irreducible representation (irrep) of the cubic group O_h. Usually, this will be the trivial A_1 representation but the smearing operator can also be used to inject angular momentum or to add nontrivial gluonic excitations [23]. Obviously, $F_{(\boldsymbol{k})}$ with a momentum shift $\boldsymbol{k} \neq \boldsymbol{0}$ breaks the cubic symmetry. However, when used in conjunction with a momentum projection that selects hadrons with a momentum $\boldsymbol{p}$, then as long as $\boldsymbol{k} \parallel \boldsymbol{p}$, the smearing operator remains within the A_1 representation of the O_h little group corresponding to the momentum direction $\boldsymbol{p}$.

III. MOMENTUM SMEARING AND HADRONIC TWO-POINT FUNCTIONS

We recapitulate Wuppertal smearing as a generic example of an iterative smearing algorithm. Then to clarify notations we discuss the standard construction of hadronic two-point functions, before generalizing the smearing by introducing a momentum shift as described above. The discussion can easily be extended to incorporate generic hadrons and n-point functions with $n \geq 2$. We conclude with a suggestion how to further improve the method. This is relevant for fine lattices where the iteration count becomes large. In the Appendix we discuss how an additional Lorentz boost factor can be implemented.

A. Wuppertal smearing

The most prominent gauge covariant realization of a smearing function is Wuppertal smearing [17,18], where $F = \Phi^n$, with Φ being defined as

$$(\Phi q)_{\boldsymbol{x}} = \frac{1}{1+2d\varepsilon}\left[q_{\boldsymbol{x}} + \varepsilon\sum_{j=\pm1}^{\pm d} U_{\boldsymbol{x},j}q_{\boldsymbol{x}+\hat{\boldsymbol{\jmath}}}\right]. \tag{9}$$

Again $d = 3$ denotes the dimension of space. The gauge transporters

$$U_{x,-j} = U^\dagger_{x-\hat{\boldsymbol{\jmath}},j}, \qquad U_{\boldsymbol{x},j} = U_{x,j} \quad \text{with} \quad x_4 \text{ fixed}, \tag{10}$$

can also be spatially APE smeared links [13,19,22]. $\hat{\boldsymbol{\jmath}}$ denotes a vector of length of one lattice unit a, pointing into the direction j. In Eq. (9) we suppressed the index x_4 since the smearing is diagonal in time. ε is a positive constant and the arbitrary normalization factor $1/(1+2d\varepsilon)$ is introduced to avoid a numerical overflow for large iteration counts n.

Φ (and by implication Φ^n) is self-adjoint, a unit matrix in spinor space and transforms according to the A_1 representation of O_h or its little groups.[1] The replacement $q \mapsto \Phi^n q$ will therefore not interfere with the symmetry properties of any interpolator.

The smearing operator Φ is related to a discretized covariant Laplacian Δ:

$$\Phi q = q + \frac{\varepsilon}{1+2d\varepsilon}a^2\Delta q, \tag{11}$$

[1] O_h symmetry will be reduced to C_{nv} for momenta along a lattice axis (C_{4v}), a spatial diagonal (C_{3v}) or a planar diagonal (C_{2v}), see, e.g., Ref. [34].

$$a^2(\Delta q)_{\boldsymbol{x}} = -2dq_{\boldsymbol{x}} + \sum_{j=\pm 1}^{\pm d} U_{\boldsymbol{x},j} q_{\boldsymbol{x}+\hat{\boldsymbol{\jmath}}}. \tag{12}$$

Introducing a fictitious time $\tau = n\Delta\tau$ and defining $q(\tau) = \Phi^n q(0)$, i.e. $q(\tau+\Delta\tau) = \Phi q(\tau)$, results in the diffusion (or heat) equation

$$\frac{\partial q(\tau)}{\partial \tau} \approx \frac{q(\tau+\Delta\tau) - q(\tau)}{\Delta\tau} = \alpha \Delta q(\tau), \tag{13}$$

where

$$\alpha = \frac{a^2}{\Delta\tau} \frac{\varepsilon}{1+2d\varepsilon}. \tag{14}$$

This is solved by $q(\tau) \approx \exp(\alpha\tau\Delta) q(0)$. Starting from δ-sources in position and color space $q^a_{\boldsymbol{x}}(0) = \delta_{\boldsymbol{x}\boldsymbol{0}}\delta^{ab}$, assuming the free case $U_{\boldsymbol{x},j} = \mathbb{1}_3$ and large distances $r = |\boldsymbol{x}| \gg a$, Eq. (13) is obviously solved by a Gaussian with

$$\sigma(\tau) = \sqrt{2\alpha\tau} = \sqrt{2na^2}\sqrt{\frac{\varepsilon}{1+2d\varepsilon}} \tag{15}$$

being the square root of the variance, i.e. the smearing corresponds to the smearing kernel Eq. (4). Employing a parallel transporter within the covariant Laplacian Eqs. (10) and (12) that is close to unity, like d dimensional APE smeared gauge links, means that this Gaussian shape is a good approximation, see, e.g., Ref. [35].

The diffusivity α obviously is maximal for large values of the parameter ε ($\alpha \to \frac{1}{6}a^2/\Delta\tau$ for $\varepsilon \to \infty$). For small values ($\alpha \approx \varepsilon a^2/\Delta\tau$), the iteration count n to achieve a given smearing radius[2] $\sqrt{3}\sigma$ is larger but the resulting wave function will be smoother. Equation (15) highlights that, to keep the smearing radius fixed in physical units, the iteration count needs to be increased in proportion to the square of the inverse lattice spacing. Obviously, this becomes computer time intensive toward the continuum limit. We remark that at small lattice spacings the diffusion equation (13) should be solved using a smarter method than iteratively applying the smearing operator Φ defined in Eq. (10). We will return to this in Sec. III E.

B. Construction of two-point functions

As an example we discuss the construction of momentum projected pion and nucleon two-point functions:

$$\begin{aligned} C_\pi(\boldsymbol{p},t) &= \langle \pi_{\boldsymbol{p}}(t)\pi^\dagger_{\boldsymbol{p}}(0)\rangle, \\ C_N(\boldsymbol{p},t) &= \langle N^\alpha_{\boldsymbol{p}}(t)\bar{N}^\beta_{\boldsymbol{p}}(0)\rangle \mathbb{P}^{\alpha\beta}, \end{aligned} \tag{16}$$

where $\mathbb{P} = \frac{1}{2}(\mathbb{1}+\gamma_4)$ denotes a projector onto positive parity.[3] Without smearing the pion and nucleon interpolators are local quark bilinears and trilinears:

$$\pi_{\boldsymbol{p}} = a^3 \sum_{\boldsymbol{x}} e^{i\boldsymbol{p}\cdot\boldsymbol{x}} \bar{u}_{\boldsymbol{x}} \gamma_5 d_{\boldsymbol{x}}, \tag{17}$$

$$N^\alpha_{\boldsymbol{p}} = a^3 \sum_{\boldsymbol{x}} e^{i\boldsymbol{p}\cdot\boldsymbol{x}} [u^t_{\boldsymbol{x}} C\gamma_5 d_{\boldsymbol{x}}] u^\alpha_{\boldsymbol{x}}, \tag{18}$$

where C is the charge conjugation operator and $u_{\boldsymbol{x}}$ and $d_{\boldsymbol{x}}$ annihilate up and down quarks, respectively, at the spatial position $\boldsymbol{x}$.

For the pion the Wick contraction then gives

$$\begin{aligned} C_\pi(\boldsymbol{p},t) &= -L^3a^3 \sum_{\boldsymbol{x}} e^{i\boldsymbol{p}\cdot\boldsymbol{x}} \langle \bar{u}_x \gamma_5 d_x d^\dagger_0 \gamma_5 \bar{u}^\dagger_0 \rangle \\ &= -L^3a^3 \sum_{\boldsymbol{x}} \langle \mathrm{tr}[(d\bar{d})_{x0}\gamma_5 (u\bar{u})_{0x}\gamma_5]\rangle e^{i\boldsymbol{p}\cdot\boldsymbol{x}} \\ &= -L^3a^3 \left\langle \sum_{\boldsymbol{x}} \mathrm{tr}(M^{-1\dagger}_{x0} M^{-1}_{x0}) e^{i\boldsymbol{p}\cdot\boldsymbol{x}} \right\rangle, \end{aligned} \tag{19}$$

where $x = (\boldsymbol{x}, t)$ and the trace is over spin and color. Momentum projection at the source is not necessary, due to the translational symmetry of expectation values and $L^3 = N^3a^3$ denotes the three-volume that corresponds to this omitted sum. M is a Wilson-like lattice Dirac matrix with the quark mass $m_u = m_d$ and we have used[4] $d^\dagger\gamma_5\bar{u}^\dagger = d^\dagger\gamma_5\gamma_4 u = -\bar{d}\gamma_5 u$, the Grassmann nature of the quark field creation and annihilation operators and replaced $\langle d\bar{d}\rangle_d = \langle u\bar{u}\rangle_u = M^{-1}$, where the subscripts d, u denote integrating out the respective Grassmann field on a given gauge background. In the last step we also exploited γ_5-Hermiticity: $\gamma_5 M^{-1}\gamma_5 = M^{-1\dagger}$. For the nucleon one can easily work out an analogous expression that contains $\epsilon^{abc}\epsilon^{a'b'c'}(M^{-1})^{aa'}_{x0}(M^{-1})^{bb'}_{x0}(M^{-1})^{cc'}_{x0}$, where we have suppressed the spinor indices and $a,b,c,a',b',c' \in \{1,2,3\}$ run over fundamental color. Equation (19) can now be evaluated, solving the linear systems

$$\sum_{x,\alpha,a} M^{\beta'b'\alpha a}_{x'x} S^{\alpha a\beta b}_x = \delta_{x'0}\delta^{b\beta'\beta}\delta^{b'b} \tag{20}$$

[2]Note that the root mean squared radius in d dimensions reads $\sqrt{d}\sigma$. Also note that the width of the gauge invariant combination $q^\dagger_{\boldsymbol{x}} q_{\boldsymbol{x}}$ Eq. (45) is smaller by a factor $\sqrt{2}$.

[3]Note that for $\boldsymbol{p} \neq \boldsymbol{0}$ this projector will not completely remove the negative parity contribution. To improve on this, instead one can employ the oblique projector [36] $\mathbb{P}_{\boldsymbol{p}} = \frac{1}{2}\{\mathbb{1} + [m_{N^*}/E_{N^*}(\boldsymbol{p})]\gamma_4\}$, where m_{N^*} and E^*_N denote mass and energy of the nucleon's negative parity partner. Since this state is higher in mass than the nucleon, for simplicity, here we abstain from attempting this.

[4]Note that the assignment $\bar{d} = d^\dagger\gamma_4$ is convenient but not consistent in Euclidean spacetime, where the Dirac operator is γ_5- instead of $(\gamma_4 = \gamma_0)$-Hermitian. This is the reason for the negative sign in Eq. (19). In the simulation, we correct for this phase and obtain a positive two-point function.

for twelve δ-sources (for each source spin β and color b) to obtain the point-to-all propagator S with sink position, spin and color indices x, α and a, respectively. Then,

$$C_\pi(\boldsymbol{p},t) \propto \left\langle \sum_{\boldsymbol{x}} \mathrm{tr}(S_x^\dagger S_x) e^{i\boldsymbol{p}\cdot\boldsymbol{x}} \right\rangle, \tag{21}$$

where again $x_4 = t$. The construction of the analogous nucleon two-point function from three point-to-all propagators is straightforward. Note that in that case no Hermitian adjoint will appear.

Smearing is diagonal in Euclidean time (hence we suppressed the t dependence) and trivial in Dirac spin. So, obviously, the smearing operator $F = \Phi^n$ commutes with any Γ structure, however, it does not commute with covariant derivatives that may appear within the hadronic interpolator. Smearing can easily be implemented at the source, replacing $S = M^{-1}\delta$ by $S^F = M^{-1}F\delta$, see Eq. (20). Note that, due to the fact that F is a unit matrix in spinor space, the same smeared source can be employed for all four spinor components. To obtain a so-called smeared-smeared two-point function, the argument of the sum in Eq. (21) will usually be replaced by $\mathrm{tr}[(FS^F)_x^\dagger (FS^F)_x] e^{i\boldsymbol{p}\cdot\boldsymbol{x}}$: every source smearing requires new inversions while sink smearing needs to be carried out on all time slices of interest.

We remark that momentum sources have been used for quite some time, see, e.g., Refs. [37–39]. Injecting momentum into quark sources is necessary (and has been done) in the context of the one-end-trick of Refs. [40,41], where one usually employs color-diagonal (complex) $\mathbb{Z}_N$ or U(1) random sources. Generalizing this to SU(3) noise is in fact equivalent to using a non-gauge fixed wall source [42], which does not change expectation values. Momentum was however also injected into gauge fixed wall sources in Refs. [27,43] ("color wave propagator"), favorably affecting not only statistical errors but also ground state overlaps. While these latter references share some of our motivation, the method presented here is quite different. For instance, in our case the hadron's total momentum still needs to be injected at the source and $\boldsymbol{k}$ is not quantized.

Finally, we remark that the asymmetry of only carrying out the position sum at the sink often is exploited to reduce the statistical errors of heavy-light meson correlation functions, by only smearing the heavy quark with $F^2 = FF$ at the source, instead of smearing each quark with F. Clearly, it would be advantageous if for each momentum smearing parameter of interest only the heavy quark propagator had to be recomputed. Unfortunately, momentum smearing (as well as traditional smearing) as an operation will not commute with momentum projection, unless $\boldsymbol{p} = \boldsymbol{0}$. Therefore, a different distribution of the smearing between the quarks will result in a different and not necessarily optimal ground state overlap.

C. Momentum (Wuppertal) smearing

As explained in Sec. II, if we inject a momentum $\boldsymbol{p}$ into the hadron, it may be a good idea to distribute at least part of it among the quarks. Their smearing functions should therefore ideally be centred around a value $\boldsymbol{k} \neq \boldsymbol{0}$, where $\boldsymbol{k}$ is some fraction of $\boldsymbol{p}$, to best resemble the wave function of the physical state we wish to create.

The Fourier transform of a Gaussian, centered about $\boldsymbol{k}$ in momentum space, reads

$$f^\sigma_{(\boldsymbol{k})\boldsymbol{x}-\boldsymbol{y}} \propto \exp\left[-\frac{(\boldsymbol{x}-\boldsymbol{y})^2}{2\sigma^2} - i\boldsymbol{k}\cdot(\boldsymbol{x}-\boldsymbol{y}) \right]. \tag{22}$$

Similarly, momentum can be injected also into differently shaped smearing functions, a possibility that we shall not explore here. $q(\tau) = F^{\sigma(\tau)}_{(\boldsymbol{k})} q(0)$ solves the heat equation with a constant drift term

$$\frac{\partial q(\tau)}{\partial \tau} = \alpha(\boldsymbol{\nabla} + i\boldsymbol{k})^2 q(\tau). \tag{23}$$

In analogy to the discussion of Sec. III A, in the free case the above smearing function can iteratively be constructed from "momentum" Gauß smearing steps, $F_{(\boldsymbol{k})} = \Phi^n_{(\boldsymbol{k})}$, introducing a phase into Eq. (9):

$$(\Phi_{(\boldsymbol{k})} q)_{\boldsymbol{x}} = \frac{1}{1+2d\varepsilon} \left[q_{\boldsymbol{x}} + \varepsilon \sum_{j=\pm 1}^{\pm d} U_{\boldsymbol{x},j} e^{i\boldsymbol{k}\hat{\jmath}} q_{\boldsymbol{x}+\hat{\jmath}} \right], \tag{24}$$

where $\Phi_{(\boldsymbol{0})} = \Phi$. One can easily show that the variance $\sigma^2(\tau)$ is still given as in Eq. (15). Moreover, as expected $\Phi_{(\boldsymbol{k})}$ remains self-adjoint:

$$\begin{aligned}
\Phi_{(\boldsymbol{k})\boldsymbol{x}\boldsymbol{y}} &= \frac{1}{1+2d\varepsilon} \Bigg\{ \delta_{\boldsymbol{x},\boldsymbol{y}} + \varepsilon \sum_{j=1}^{3} [\delta_{\boldsymbol{x}+\hat{\jmath},\boldsymbol{y}} U_{\boldsymbol{x},j} e^{i\boldsymbol{k}\hat{\jmath}} \\
&\qquad + \delta_{\boldsymbol{y}+\hat{\jmath},\boldsymbol{x}} U^\dagger_{\boldsymbol{y},j} e^{-i\boldsymbol{k}\hat{\jmath}}] \Bigg\}, \\
\Phi^\dagger_{(\boldsymbol{k})\boldsymbol{y}\boldsymbol{x}} &= \frac{1}{1+2d\varepsilon} \Bigg\{ \delta_{\boldsymbol{y},\boldsymbol{x}} + \varepsilon \sum_{j=1}^{3} [\delta_{\boldsymbol{y}+\hat{\jmath},\boldsymbol{x}} U^\dagger_{\boldsymbol{y},j} e^{-i\boldsymbol{k}\hat{\jmath}} \\
&\qquad + \delta_{\boldsymbol{x}+\hat{\jmath},\boldsymbol{y}} U_{\boldsymbol{x},j} e^{i\boldsymbol{k}\hat{\jmath}}] \Bigg\} = \Phi_{(\boldsymbol{k})\boldsymbol{x}\boldsymbol{y}}.
\end{aligned} \tag{25}$$

We will use the same smearing for quarks and antiquarks. For the π^- meson this amounts to the replacements $d \mapsto \Phi^n_{(\boldsymbol{k})} d$, $u \mapsto \Phi^n_{(-\boldsymbol{k})} u$, $\bar{d} \mapsto \bar{d}\Phi^n_{(\boldsymbol{k})}$ and $\bar{u} \mapsto \bar{u}\Phi^n_{(-\boldsymbol{k})}$ within Eq. (19). Note that the $\Phi^n_{(-\boldsymbol{k})}$ smearing is needed as in the contraction with the momentum projector, $(\delta_{\boldsymbol{x}\boldsymbol{x}'} e^{i\boldsymbol{p}\cdot\boldsymbol{x}}) \Phi^n_{(\boldsymbol{k})\boldsymbol{x}\boldsymbol{y}} \Phi^n_{(\boldsymbol{k})\boldsymbol{x}'\boldsymbol{y}'}$, transposing the ordering of the indices of the first smearing operator gives $\Phi^n_{(\boldsymbol{k})\boldsymbol{x}\boldsymbol{y}} = \Phi^n_{(-\boldsymbol{k})\boldsymbol{y}\boldsymbol{x}}$ in the free case, see Eq. (29). Exploiting the Hermiticity of $\Phi^n_{\boldsymbol{k}}$, we then obtain

$$C_\pi(t) \propto \sum_{\boldsymbol{x}} \langle \mathrm{tr}\{[(\Phi^n_{(-\boldsymbol{k})} M^{-1} \Phi^n_{(-\boldsymbol{k})})_{x0}]^\dagger (\Phi^n_{(\boldsymbol{k})} M^{-1} \Phi^n_{(\boldsymbol{k})})_{x0}\}\rangle e^{i\boldsymbol{p}\cdot\boldsymbol{x}}. \tag{26}$$

In contrast, for baryonic two-point functions, where all quarks propagate in the forward direction, only $\Phi^n_{(+\boldsymbol{k})}$ will appear. The pion two-point function can now be constructed in analogy to Eq. (21) from

$$C_\pi(\boldsymbol{p},t) \propto \left\langle \sum_{\boldsymbol{x}} \mathrm{tr}[(\Phi^n_{(-\boldsymbol{k})} S_{(-\boldsymbol{k})})^\dagger_x (\Phi^n_{(\boldsymbol{k})} S_{(\boldsymbol{k})})_x] e^{i\boldsymbol{p}\cdot\boldsymbol{x}} \right\rangle, \tag{27}$$

where the source-smeared point-to-all propagator is defined as [see Eq. (20)]

$$S_{(\boldsymbol{k})}{}^{\alpha a \beta b}_x = \sum_{x',\alpha',a',z,c} (M^{-1})^{\alpha a \alpha' a'}_{x,x'} \delta^{\alpha'\beta} \Phi^n_{(\boldsymbol{k})}{}^{a'c}_{x'z} \delta_{z0} \delta^{cb}, \tag{28}$$

or, in shorthand notation: $S_{(\boldsymbol{k})} = M^{-1}\Phi^n_{(\boldsymbol{k})}\delta$. For mesons the above twelve linear systems need to be solved, both for δ-sources smeared with $\Phi^n_{(\boldsymbol{k})}$ and with $\Phi^n_{(-\boldsymbol{k})}$, while for baryons smearing with $\Phi^n_{(\boldsymbol{k})}$ is sufficient.

We remark that the momentum smearing Eq. (24) can very easily be implemented by substituting the (APE smeared) transporters $U_{\boldsymbol{x},j} \mapsto U_{\boldsymbol{x},j} e^{i\boldsymbol{k}\hat{\boldsymbol{\jmath}}}$ and then iterating the usual Wuppertal smearing Eq. (9) on these modified U(3) links.

D. Free field investigation

Having defined the smearing and how the contractions are to be carried out, we are now in the position to address the question what value of $\boldsymbol{k}$ should be chosen. Naively, one may expect $\boldsymbol{k} \approx \boldsymbol{p}/2$ and $\boldsymbol{k} \approx \boldsymbol{p}/3$ to be optimal for mesons and baryons, respectively, that are composed of degenerate quarks and carry a total momentum $\boldsymbol{p}$. This is indeed what we will find here for the noninteracting case. The interacting case somewhat deviates from this as we will see in Sec. V below.

Setting $U_{\boldsymbol{x},j} = \mathbb{1}$ within Eq. (24) gives the free case smearing function Eq. (22) for a large volume $L^3 \gg \sigma^3$ and number of smearing iterations so that $\sigma \gg a$. Smearing the quark and antiquark annihilation operators at the sink with $F_{(\boldsymbol{k})}$ and $F_{(-\boldsymbol{k})}$, respectively, we obtain the momentum projected smeared pion interpolator,

$$\begin{aligned} \pi_{\boldsymbol{p}} &\propto \sum_{\boldsymbol{x},\boldsymbol{y},\boldsymbol{y}'} \bar{u}_{\boldsymbol{y}'} f_{(-\boldsymbol{k})\boldsymbol{y}'-\boldsymbol{x}} e^{i\boldsymbol{p}\cdot\boldsymbol{x}} f_{(\boldsymbol{k})\boldsymbol{x}-\boldsymbol{y}} \gamma_5 d_{\boldsymbol{y}} \\ &\propto \sum_{\boldsymbol{x},\boldsymbol{y},\boldsymbol{y}'} \exp\left[-\frac{(\boldsymbol{y}-\boldsymbol{x})^2 + (\boldsymbol{y}'-\boldsymbol{x})^2}{2\sigma^2}\right] e^{i\boldsymbol{p}\cdot\boldsymbol{x}} e^{-2i\boldsymbol{k}\cdot\boldsymbol{x}} e^{i\boldsymbol{k}\cdot(\boldsymbol{y}+\boldsymbol{y}')} [\bar{u}_{\boldsymbol{y}'}\gamma_5 d_{\boldsymbol{y}}] \\ &\propto \exp\left[-\frac{\sigma^2}{2}(\boldsymbol{p}-2\boldsymbol{k})^2\right] \sum_{\boldsymbol{Z},\boldsymbol{\Delta}} \exp\left[-\frac{\boldsymbol{\Delta}^2}{\sigma^2}\right] e^{i\boldsymbol{p}\cdot\boldsymbol{Z}} [\bar{u}_{\boldsymbol{Z}+\boldsymbol{\Delta}}\gamma_5 d_{\boldsymbol{Z}-\boldsymbol{\Delta}}], \end{aligned} \tag{29}$$

where we have defined center and relative coordinates

$$\boldsymbol{Z} = \frac{\boldsymbol{y}+\boldsymbol{y}'}{2}, \qquad \boldsymbol{\Delta} = \frac{\boldsymbol{y}'-\boldsymbol{y}}{2}. \tag{30}$$

Note that the components of $\boldsymbol{Z}/a$ and $\boldsymbol{\Delta}/a$ can be integer or half-integer valued, subject to the constraints $(Z_j + \Delta_j)/a \in \mathbb{Z}$. The result of Eq. (29) is indeed maximized for $\boldsymbol{k} = \boldsymbol{p}/2$: in the free case $\boldsymbol{k} = \boldsymbol{p}/2$ is the optimal smearing parameter for mesons with mass-degenerate valence quarks while we encounter an exponential suppression in $\boldsymbol{p}^2$ for the conventional $\boldsymbol{k} = \boldsymbol{0}$ smearing. The broader the wave function in coordinate space, the more important becomes the correct choice of $\boldsymbol{k}$ as one can see from the first exponent in Eq. (29) [as well as from Eq. (5)]. Unsurprisingly, for baryonic interpolators $\boldsymbol{k} = \boldsymbol{p}/3$ would be the optimal choice.

We have demonstrated that in the free case $\boldsymbol{k}$ can be interpreted as the momentum carried by the smeared quark. If the quarks differ in mass or, like for the example of the nucleon, the interpolator is not symmetric with respect to the quark flavor, injecting different $\boldsymbol{k}$-values into different quark fields may be advisable. In the interacting case the interpretation is not as straightforward: neither is the interpolator directly related to any of the usual definitions of a wave function nor will all momentum be carried by the valence quarks.

E. Noniterative (momentum) smearing

We propose replacing iterative smearing, where the iteration count diverges with a^{-2} toward the continuum limit, by a more refined method. In this context we show how to introduce phase factors (and shape functions) into the "distillation" (or Laplacian-Heaviside) method of Ref. [31]. Although we already present the basics of the method here, systematic tests are yet to be completed. Another natural extension, which we will investigate numerically in Sec. V, is to Lorentz boost the smearing function.

We define eigenvectors $|v_\ell\rangle$ and eigenvalues $-\omega_\ell^2$ of a covariant Laplacian with (smeared) gauge transporters, at a fixed Euclidean time:

$$(\Delta + \omega_\ell^2)|v_\ell\rangle = 0. \tag{31}$$

Since the Laplacian is self-adjoint, the bra-ket notation is convenient in the present context. For a lattice of N^d points per time slice ($L = Na$), $3N^d$ linearly independent eigenvectors $|v_\ell\rangle$ with components $v^a_{\ell \boldsymbol{x}}$ exist. Such eigenvectors were for instance used in Ref. [31]. The heat equation (13) is solved by

$$\begin{aligned} |q(\tau)\rangle &= \exp(\alpha\tau\Delta)|q(0)\rangle \\ &= \sum_\ell |v_\ell\rangle \exp(-\alpha\tau\omega_\ell^2)\langle v_\ell|q(0)\rangle. \end{aligned} \tag{32}$$

If we start from a δ-function at $\tau = 0$, this results in a Gaussian of variance $\sigma^2 = 2\alpha\tau$.

To implement momentum smearing one can easily replace $U_{\boldsymbol{x},j} \mapsto U_{\boldsymbol{x},j} e^{i\boldsymbol{k}\hat{\boldsymbol{\jmath}}}$ within the covariant Laplacian $\Delta \mapsto \Delta_{(\boldsymbol{k})} \sim (\boldsymbol{\nabla} + i\boldsymbol{k})^2$ and then recompute the eigenvectors and -values:

$$(\Delta_{(\boldsymbol{k})} + \omega^2_{(\boldsymbol{k})\ell})|v_{(\boldsymbol{k})\ell}\rangle = 0. \tag{33}$$

The natural generalization of Eq. (32) for moving particles then reads:

$$|q_{(\boldsymbol{k})}(\tau)\rangle = \sum_\ell |v_{(\boldsymbol{k})\ell}\rangle \exp(-\alpha\tau\omega^2_{(\boldsymbol{k})\ell})\langle v_{(\boldsymbol{k})\ell}|q(0)\rangle. \tag{34}$$

The motivation for computing eigenvectors of the covariant Laplacian is to truncate Eqs. (32) or (34) at a value $\ell_{\max}$ where $\omega^2_{\ell_{\max}+1} > \omega^2_{\max}$. As $\alpha\tau = \sigma^2/2$, achieving a suppression by a factor e^{-2} requires $\omega_{\max} \approx 2/\sigma$. In general, the wider the smearing function in coordinate space the less eigenvectors will be needed. The extreme opposite limit $\alpha\tau = 0 \Rightarrow \sigma = 0$ corresponds to the Laplacian-Heaviside method proposed in Ref. [31], where summing over all eigenvectors will ultimately result in a δ-function in position space while truncating at some finite $\ell_{\max}$ value gives a bell shape [31]. (In the free case the modulus would be a sum of sines.) The same holds for the sources suggested in Ref. [38] that correspond to sums of eigenvectors of the noninteracting Laplacian.

It is trivial to work out more details in the free case, where one basically encounters a one dimensional problem. For instance, setting $\omega = j(2\pi/L) \gtrsim 2/\sigma$, where $j \in \mathbb{Z}\backslash\{0\}$ means $|j| \gtrsim L/(\pi\sigma)$. Therefore, in d dimensions $\ell_{\max} \gtrsim 3 \times [\pi^{d/2}/\Gamma(d/2+1)] \times [L/(\pi\sigma)]^d$, where the factor 3 is due to color and the next factor is the volume of a d dimensional unit-sphere ($4\pi/3$ for $d = 3$): the number of required eigenvectors increases in proportion to the spatial volume in physical units but is independent of the lattice spacing a. In contrast, in the case of iterative smearing, reducing the lattice spacing at a fixed value of σ increases the iteration count in proportion to a^{-2}, independent of the volume. For our smearing size $\sigma \approx 0.45$ fm and a spatial volume $L^3 = (6\text{ fm})^3$, which would ensure $Lm_\pi > 4$ even at the physical mass point, we obtain $\ell_{\max} \approx 960$ while for a $(3\text{ fm})^3$ box about 120 eigenvectors should suffice. Therefore, satisfactory results in terms of ground state overlaps appear to be within reach, employing moderately large numbers of eigenvectors. This is at present under investigation.

Non-Gaussian shapes can easily be modeled too, e.g., by multiplying in a "free form" weight function, $(|v_\ell\rangle\langle v_\ell|)_{\boldsymbol{xy}} \mapsto \sum_{\boldsymbol{xy}} h_{\boldsymbol{xy}} \exp[\alpha\tau(\boldsymbol{x}-\boldsymbol{y})^2](|v_\ell\rangle\langle v_\ell|)_{\boldsymbol{xy}}$, in analogy to Ref. [25]. However, the numerical complexity of this operation is $\mathcal{O}(N^{2d})$ for each time slice and eigenvector. At the source this can be reduced to $\mathcal{O}(N^d)$ if the solution is only required for a fixed δ-source position $|q(0)\rangle = |\delta^a_{\boldsymbol{y}_0}\rangle$ ($(\langle \boldsymbol{y}, b|\delta^a_{\boldsymbol{y}_0}\rangle = (|\delta^a_{\boldsymbol{y}_0}\rangle)^b_{\boldsymbol{y}} = \delta_{\boldsymbol{y}\boldsymbol{y}_0}\delta^{ba}$). Other, numerically less expensive options include placing nonlinear functions of ω^2_ℓ in the exponents of Eqs. (32) and (34), employing linear combinations of Gaussians or substituting the covariant Laplacian by a different operator within Eqs. (31) and (33), e.g., introducing an anisotropy.

Once the eigenvectors Eq. (31) or Eq. (33) of the APE or HYP smeared covariant Laplacian have been computed, any smearing radius can be realized, replacing $\alpha\tau$ by the targeted $\sigma^2/2$ value within the exponent of Eq. (32) or Eq. (34). Another potential advantage of the non-iterative smearing is that, instead of solving for smeared sources $|q_{(\boldsymbol{k})}(\tau)\rangle$ that have evolved from a δ-source $|q(0)\rangle = |\delta_{\boldsymbol{y}_0 a}\rangle$, one can also directly apply the inverse lattice Dirac operator to the eigenvectors, thereby constructing so-called perambulators [31]:

$$\tau^{\alpha\beta}_{(\boldsymbol{k})mt\ell 0} = \langle v_{(\boldsymbol{k})mt}|(M^{-1})^{\alpha\beta}_{t0}|v_{(\boldsymbol{k})\ell 0}\rangle. \tag{35}$$

The inner product above is over spatial position and color, replacing these indices by the eigenvector labels ℓ at the sink and m at the source. The respective Euclidean times are explicitly shown as additional eigenvector (and perambulator) subscripts. These perambulators can then be folded with the appropriate eigenvalue Gaussians during the construction of hadronic n-point functions.

We abstain from repeating here the steps outlined in Ref. [31] how to construct hadronic two-point functions from these perambulators as there is only one difference: In the contractions over ℓ and m weight factors $\exp(-\sigma^2\omega^2_{(\boldsymbol{k})\ell 0}/2)$ and $\exp(-\sigma^2\omega^2_{(\boldsymbol{k})mt}/2)$ should be introduced, where $\omega^2_{(\boldsymbol{k})mt}$ refers to the mth eigenvalue of the negative covariant Laplacian defined on time slice t.

On one hand using perambulators will require a larger number of inversions and computationally more expensive contractions than starting from δ-sources. On the other hand, due to volume averaging, the statistical errors of the perambulator method will be smaller and this method allows for more flexibility in the subsequent construction

of hadronic n-point functions. Whether the use of perambulators or of traditional (smeared) point-to-all propagators is preferable will therefore depend on the problem at hand and in particular on the number of different hadrons we are interested in. We have shown that the same quark smearing can be employed in both cases.

Finally, we remark that in certain situations recomputing the eigenvectors for different values of $\boldsymbol{k}$ may be avoidable. In the interacting case, gauge covariant derivatives ∇_j^2 will depend on all spatial coordinates, including x_i with $i \neq j$, and will therefore not commute with each other. However, our intuition was based on the free case and also the spatially APE [13] or HYP [15] smeared gauge covariant transporters are close to unity. Assuming translational invariance, the coordinates can be separated and the components of an eigenvector read $v_{\boldsymbol{x}}^a \propto \sin(\omega_1^a x_1)\cdots \sin(\omega_d^a x_d)$, where $\omega_j^a = 2\pi m_j^a/L$ and m_j^a are integer valued. The corresponding eigenvalue of the negative Laplacian is given as $\omega^2 = \boldsymbol{\omega}^2$ where the frequencies for different color components are constrained: $\boldsymbol{\omega}^2 \coloneqq \boldsymbol{\omega}^{12} = \boldsymbol{\omega}^{22} = \boldsymbol{\omega}^{32}$. Defining

$$|\tilde{v}_{(\boldsymbol{k})\ell}\rangle = e^{-i\boldsymbol{k}\cdot\boldsymbol{x}}|v_\ell\rangle \tag{36}$$

then gives $[(\boldsymbol{\nabla} + i\boldsymbol{k})^2 + \omega_\ell^2]|\tilde{v}_{(\boldsymbol{k})\ell}\rangle = 0$.

In the interacting case this will not exactly solve the heat equation with drift (23) but the approximation $\omega_{(\boldsymbol{k})\ell} \approx \omega_\ell$, $|v_{(\boldsymbol{k})\ell}\rangle \approx |\tilde{v}_{(\boldsymbol{k})\ell}\rangle$ should be sufficient to construct a gauge covariant Gaussian shape with the intended phase factors. Note that the phases Eq. (36) appear both in the bra- and in the ket-vector of Eq. (34), such that only relative phases between two spatial positions matter and the choice of the zero point becomes irrelevant. The clear disadvantage of the explicit multiplication by phase factors Eq. (36) is that these have to obey the lattice periodicity, i.e. $k_j \in (2\pi/L)\mathbb{Z}$. However, such a restriction may be tolerable on large lattices. Also introducing twisted fermionic boundary conditions [44,45] may provide a way to increase the flexibility of the choice of $\boldsymbol{k}$.

IV. LATTICE ENSEMBLE AND DISPERSION RELATIONS

We study the new momentum smearing method on 200 effectively decorrelated configurations of $N_f = 2$ nonperturbatively improved Wilson fermions with the Wilson gluon action, generated by QCDSF and RQCD. This constitutes a subset of ensemble IV of Ref. [46]. Note that in hadron structure studies we typically employ several sources on about 2000 configurations [46], i.e. the present statistics are very moderate. Nevertheless, we will report meaningful signals for momenta as high as 2.8 GeV. The parameter values of this $32^3 \times 64$ ensemble read $\beta = 5.29$, $\kappa = 0.13632$, corresponding to the inverse lattice spacing $a^{-1} \approx 2.76$ GeV and the (finite volume) pion mass $m_\pi \approx 295$ MeV. This gives a spatial extent $L \approx 2.29\ \text{fm} \approx 3.42/m_\pi$. Note that realizing the physical pion mass at this lattice spacing, while keeping $L \gtrsim 3.5/m_\pi$, requires $L > 70a$. As we are aiming at momenta exceeding the hadron masses in any case, we do not expect qualitative changes of results towards smaller pion masses and have chosen the present parameters as a sufficiently realistic but still affordable compromise.

The momentum on a finite cubic lattice with even numbers of points $N = L/a$ in each spatial direction can take the discrete values

$$\boldsymbol{p} = \frac{2\pi}{L}\boldsymbol{P}, \qquad P_i \in \left\{-\frac{L}{2a}+1, -\frac{L}{2a}+2, \ldots, \frac{L}{2a}\right\}. \tag{37}$$

This means the smallest nontrivial $|\boldsymbol{P}| = |(1,0,0)|$ gives a momentum $|\boldsymbol{p}| \approx 0.54\,\text{GeV}$ while $\boldsymbol{P} = (3,3,3)$ corresponds to $|\boldsymbol{p}| \approx 2.82$ GeV.

The pion and nucleon masses have already been determined with high statistics in Ref. [47] and read

$$am_\pi = 0.10675(52), \qquad am_N = 0.3855(45). \tag{38}$$

We will compare our pion and nucleon ground state energies to expectations from continuum and lattice dispersion relations, using these reference values. The continuum dispersion relation reads

$$aE = a\sqrt{m^2 + \boldsymbol{p}^2}. \tag{39}$$

In addition, we will compare the pion energies to the lattice dispersion relation for a free naively discretized scalar particle,

$$\cosh(aE_\pi) = \cosh(am_\pi) + \frac{a^2}{2}\hat{\boldsymbol{p}}^2, \tag{40}$$

and the nucleon energies to the dependence expected for a free Wilson fermion with the Wilson parameter $r = 1$, see, e.g., Ref. [48],

$$\cosh(aE_N) = 1 + \frac{(e^{am_N} - 1 + a^2\hat{\boldsymbol{p}}^2/2)^2 + a^2\bar{\boldsymbol{p}}^2}{2(e^{am_N} + a^2\hat{\boldsymbol{p}}^2/2)}. \tag{41}$$

Above, we used the standard abbreviations

$$\hat{p}_\mu = \frac{2}{a}\sin\left(\frac{ap_\mu}{2}\right), \qquad \bar{p}_\mu = \frac{1}{a}\sin(ap_\mu), \tag{42}$$

and $\hat{\boldsymbol{p}}^2 = \sum_j \hat{p}_j^2$, $\bar{\boldsymbol{p}}^2 = \sum_j \bar{p}_j^2$. We remark that the mass parameters m_0 within the naive propagators (e.g., for the scalar case: $1/(m_0^2 + \hat{p}_\mu\hat{p}_\mu)$) differ from the rest frame energies by lattice artefacts. The above masses are defined

to satisfy $m = E(\mathbf{0})$, as it should be. Their conversions to m_0 are given as $m_\pi = 2a^{-1}\sinh(am_0/2)$ and $m_N = a^{-1}\ln(1+am_0)$, respectively.

Obviously, the continuum dispersion relation should become violated toward large momenta. In this case, we would not expect the lattice dispersion relations, that apply to free pointlike particles, to accurately describe the data either. However, the difference between the continuum and the lattice formulas can serve as a naive estimate of the expected size of lattice artefacts.

V. RESULTS

We first describe and check our implementation of momentum Wuppertal smearing. Then, in Sec. V B we optimize the smearing parameters and test the effectiveness of the method. In Sec. V C we investigate whether introducing an additional Lorentz contraction is advantageous, before determining pion and nucleon dispersion relations up to momenta of 1.94 GeV and 2.82 GeV, respectively, in Sec. V D.

A. Implementation of the smearing

We iterate the momentum Wuppertal smearing on our $d+1=3+1$ dimensional gauge ensemble described in Sec. IV, employing spatially APE smeared [13] gauge transporters within Eq. (24). These are iteratively constructed as follows.

$$U^{(n+1)}_{\boldsymbol{x},i} = P_{\mathrm{SU}(3)}\left(U^{(n)}_{\boldsymbol{x},i} + \delta\sum_{|j|\neq i} U^{(n)}_{\boldsymbol{x},j}U^{(n)}_{\boldsymbol{x}+\hat{\boldsymbol{\jmath}},i}U^{(n)\dagger}_{\boldsymbol{x}+\hat{\boldsymbol{\imath}},j}\right), \quad (43)$$

where $i\in\{1,2,3\}$, $j\in\{\pm1,\pm2,\pm3\}$: the sum is over the four spatial "staples," surrounding $U_{\boldsymbol{x},i}$ where, again, we suppressed the time index as the smearing is local in time. $P_{\mathrm{SU}(3)}$ is a gauge covariant projector onto the SU(3) group, defined by maximizing $\mathrm{Retr}[A^\dagger P_{\mathrm{SU}(3)}(A)]$. We iterate over the three diagonal SU(2) subgroups to achieve this. Other projection possibilities can, e.g., be found in Refs. [22,49]. We iterate Eq. (43) 15 times, using the weight factor $\delta = 2.5$.

Momentum Wuppertal smearing Eq. (24) is implemented, multiplying the APE smeared links for a given $\boldsymbol{k}$ value by phases, $U_{\boldsymbol{x},j}\mapsto U_{\boldsymbol{x},j}e^{i\boldsymbol{k}\cdot\hat{\boldsymbol{\jmath}}}$, and then iterating the usual Wuppertal smearing Eq. (9) on these links. Within this article we set $\varepsilon = 0.25$ to obtain smooth smearing functions at tolerable iteration counts. Starting from three δ-functions (one for each source color b) at the spatial position $\mathbf{0}$, we can define "wave functions" for three different source colors,

$$\psi^{ab}_{(\boldsymbol{k})\boldsymbol{x}} = \sum_{\boldsymbol{x}',a'}(\Phi^n_{(\boldsymbol{k})})^{aa'}_{\boldsymbol{x}\boldsymbol{x}'}\delta^{a'b}_{\boldsymbol{x}'\mathbf{0}}, \quad (44)$$

and the associated gauge invariant density:

$$\rho(\boldsymbol{x}) = \frac{\sum_{ab}|\psi^{ab}_{(\boldsymbol{k})\boldsymbol{x}}|^2}{a^3\sum_{\boldsymbol{x},ab}|\psi^{ab}_{(\boldsymbol{k})\boldsymbol{x}}|^2}. \quad (45)$$

$\rho(\boldsymbol{x})$ does not carry any information relating to the U(1) phases. We therefore define

$$\varphi(\boldsymbol{x}) = \arg\left(\frac{\psi^{11}_{(\boldsymbol{k})\boldsymbol{x}}}{\psi^{11}_{(\mathbf{0})\boldsymbol{x}}}\right)\in[0,2\pi), \quad (46)$$

as the phase of momentum smearing, relative to the standard Wuppertal smearing. Above, we have singled out one particular color component but any diagonal component will give the same phase function $\varphi(\boldsymbol{x})$. In the case of a free configuration, i.e. employing trivial links $U_{\boldsymbol{x},i}=\mathbb{1}$, Eqs. (45)–(46) simplify since $\psi^{11}_{(\boldsymbol{k})\boldsymbol{x}}=\psi^{22}_{(\boldsymbol{k})\boldsymbol{x}}=\psi^{33}_{(\boldsymbol{k})\boldsymbol{x}}$ and color off-diagonal elements vanish. Moreover, $\varphi(\boldsymbol{x}) = \arg(\psi^{11}_{(\boldsymbol{k})\boldsymbol{x}})$ in this case.

In Fig. 2 we display $\rho(\boldsymbol{x})$ in lattice units for the two dimensional cross section $x_3 = 0$ and different settings. The color encodes the phase $\varphi(\boldsymbol{x})$. We employ $n = 200$ momentum Wuppertal smearing iterations with $\varepsilon = 0.25$ and set $\boldsymbol{K} = (1,1,0) = [L/(2\pi)]\boldsymbol{k}$, i.e. $\boldsymbol{k}$ lies within the depicted plane and its modulus is given as $|\boldsymbol{k}|\approx 0.77$ GeV. Up to discretization and finite volume effects, with this smearing we expect the free case variance $\sigma^2\approx(6.3a)^2$ from Eq. (15), i.e. $\rho(|\boldsymbol{x}|=6.3a)\approx e^{-1}\rho(0)$. In the top left panel we show the free case result from our iterative smearing, which is consistent with this expectation. In the top right panel of Fig. 2 we repeat this on one time slice of one of our gauge configurations, after having APE smeared the gauge links. The resulting shape is slightly narrower but otherwise indistinguishable from the free case and almost invariant with respect to continuous rotations. However, rotations take place in color space: plotting individual components of $q^{ab}_{\boldsymbol{x}}$ (not shown) gives a less smooth behavior. In particular, the off-diagonal components do not vanish anymore. The smoothness of the gauge invariant density $\rho(\boldsymbol{x})$ means that the differences relative to the free case can be removed almost completely by a suitable gauge transformation.

In the bottom left panel we apply momentum Wuppertal smearing to a time slice of the original, not APE smeared gauge links. In this case the resulting density is less symmetric and less smooth. As one may expect from mean field arguments [50], the average smearing radius is somewhat reduced in a way consistent with multiplying ε by the fourth root of the average plaquette. Also in this case, the U(1) phase information is intact. A comparison with the top right panel of Fig. 2 clearly demonstrates the advantage of additional gauge link smearing.

Finally, in the lower right panel we apply boosted momentum Wuppertal smearing Eqs. (A6)–(A8), using the APE smeared gauge links. We set $\gamma = 5.3$, which

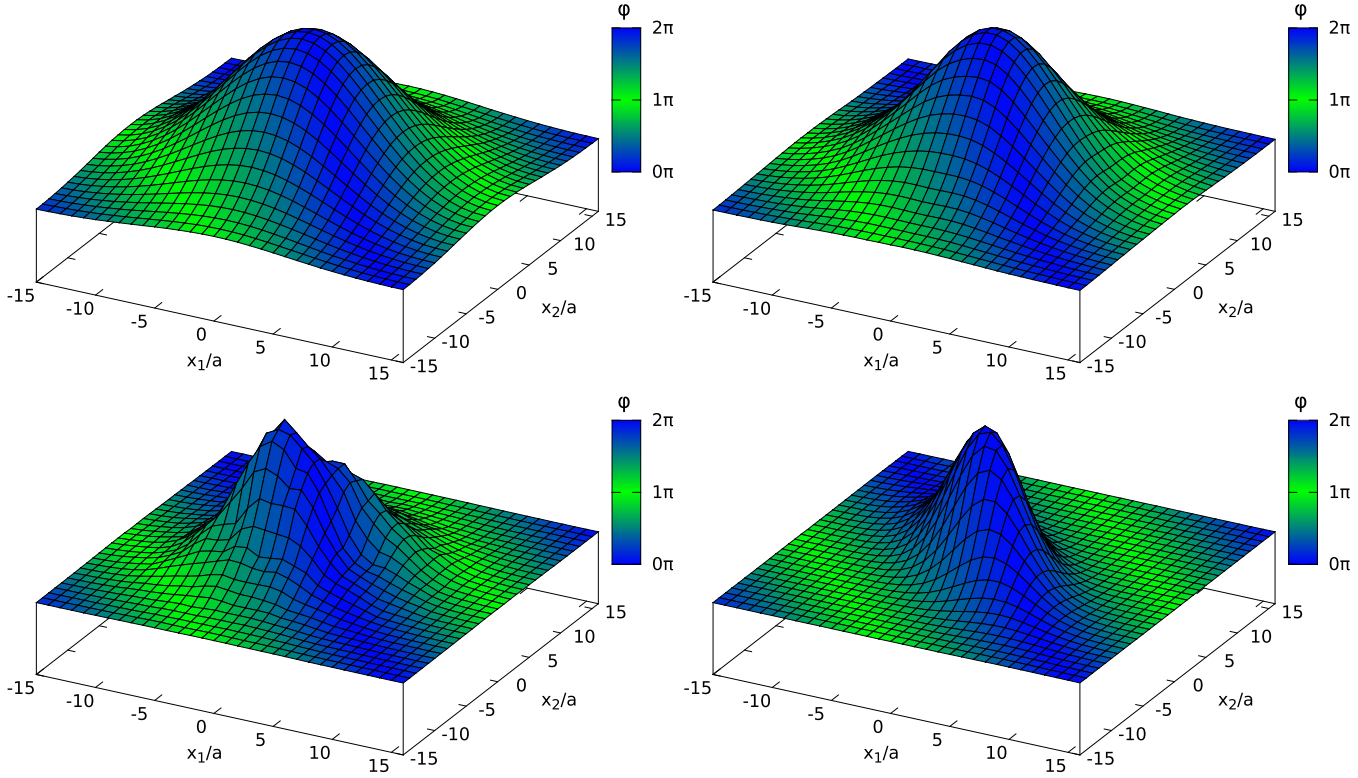

FIG. 2. Cross sections of the smearing density profile $\rho(\boldsymbol{x})$ Eq. (45) in the $x_1 - x_2$ plane. The color encodes the phase Eq. (46) and the momentum smearing $\boldsymbol{k}$ parameter has the direction (1,1,0). Top left: free field case. Top right: APE smeared gauge links. Bottom left: original gauge links. Bottom right: APE smeared links with an additional boost factor $\gamma = 5.3$.

corresponds to the ratio of the pion energy for a momentum $\boldsymbol{p} \approx 2\boldsymbol{k}$ over the pion mass $m_\pi = 295$ MeV. The smearing parameter is converted according to Eq. (A10). Indeed, the perpendicular shape in the central region is basically unaltered relative to the top panels while in the direction parallel to the boost the density is contracted by the γ factor. Due to the large numerical value of this factor there are slight deviations from the theoretical expectation but these discretization related effects can be removed by reducing the smearing parameter ε' and increasing the iteration count n, keeping σconstant, see Eqs. (15) and (A10).

B. Optimization and test of momentum smearing

We now compute smeared-point and smeared-smeared pion and nucleon two-point functions at different lattice momenta Eq. (37), where we denote momentum and smearing vectors in physical units as $\boldsymbol{p}$ and $\boldsymbol{k}$, respectively, and integer component lattice momenta as $\boldsymbol{P} = [L/(2\pi)]\boldsymbol{p}$. Note that $\boldsymbol{K} = [L/(2\pi)]\boldsymbol{k}$ does not need to have integer valued components. We (mostly) restrict ourselves to

$$\boldsymbol{K} = \zeta \boldsymbol{P}, \tag{47}$$

where the naive expectation would be $\zeta = 1/2$ for the pion and $\zeta = 1/3$ for the nucleon, see Sec. III D. From the resulting two-point functions, we define effective energies

$$E_{H,\mathrm{eff}}(\boldsymbol{p}, t + a/2) = \frac{1}{a} \ln\left[\frac{C_H(\boldsymbol{p}, t)}{C_H(\boldsymbol{p}, t + a)}\right], \tag{48}$$

where $H \in \{\pi, N\}$. For the nonperturbatively improved action that we use, which contains a clover term that couples adjacent time slices, the meaningful range of t values is $t \geq 2a$, i.e. we plot effective energies, starting at $2.5a \approx 0.18$ fm.

We realized different numbers of iteration counts n both for momentum and for conventional Wuppertal smearing. In both cases the best results in terms of the ground state overlaps for pions and nucleons at different momenta were obtained within the range $200 \lesssim n \lesssim 400$. For the results we present here we set $n = 200$, $\varepsilon = 0.25$, corresponding to $\sigma \approx 6.3a \approx 0.45$ fm, see Fig. 2. We average the pion two-point function propagating in the forward and backward time directions (folding). For the nucleon we can only make use of the forward correlation function, since we only employed the projector $\mathbb{P} = \frac{1}{2}(\mathbb{1} + \gamma_4)$, see Eq. (16).

In Fig. 3 we show effective energies from smeared-smeared two-point functions for different values of ζ. In this case $\zeta = 0.8$ (red squares) appears to be the best choice, however the results are relatively robust against increasing or decreasing this by 20%. In general, at our pion mass $m_\pi \approx 295$ MeV and momenta up to ~3 GeV, the optimal ζ values came out to be $\zeta \approx 0.8 > 1/2$ for the pion

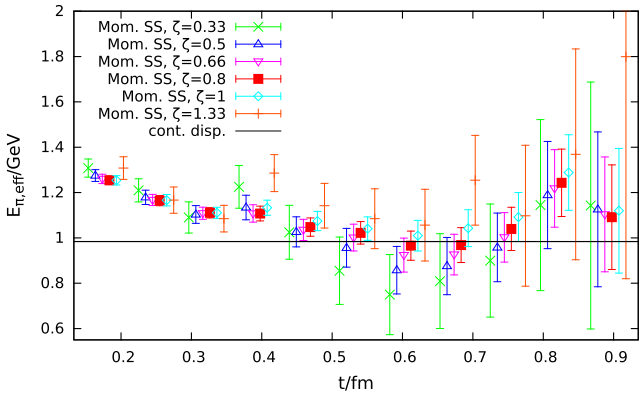

FIG. 3. Effective pion energies for $\boldsymbol{P} = (1,1,0)$, corresponding to $|\boldsymbol{p}| \approx 0.94$ GeV and different ratios ζ, see Eq. (47). The line is the expectation from the continuum dispersion relation. Symbols are shifted horizontally to enhance the legibility.

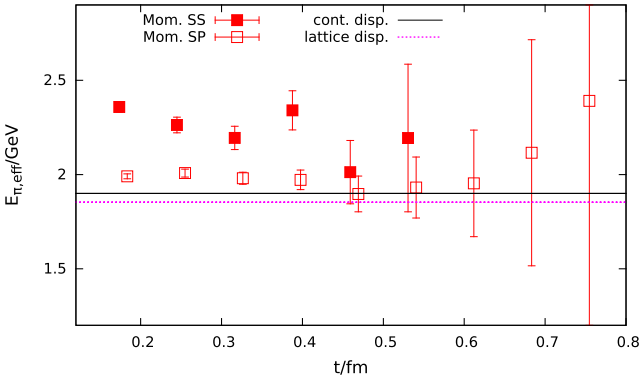

FIG. 5. The same as Fig. 4 for $\boldsymbol{P} = (1,1,1)$, corresponding to $|\boldsymbol{p}| \approx 1.88$ GeV. The effective energies without momentum smearing cannot be determined, due to prohibitively large errors and nonmonotonous behavior of the central values of the respective two-point functions.

and $\zeta \approx 0.45 > 1/3$ for the nucleon. As discussed in Sec. III D, we can only interpret $\boldsymbol{k}$ as the momentum carried by a single quark in the noninteracting case. Nevertheless, finding values that are larger than the naive expectation, rather than smaller, was somewhat unexpected. Since the deviation from the free field case is not uniform but bigger for the pion than for the nucleon, it would be interesting to extend our study to non-Gaussian smearing functions.

In Figs. 4 and 5 we compare effective pion energies from smeared-point (SP) and smeared-smeared (SS) correlation functions with the expectations from the continuum and lattice dispersion relations Eqs. (39) and (40), using the pion mass Eq. (38) (horizontal lines). Note that the SS effective energies should be monotonous functions of t while this need not be the case for SP energies. It is well known that statistical errors of SP correlators are smaller than in the SS case and we also confirm this. For the momentum smeared two-point functions the data are consistent with plateaus for $t \gtrsim 0.5$ fm and we find agreement with the expectations. For $|\boldsymbol{p}| \approx 0.94$ GeV (Fig. 4) also the effective energies from conventionally smeared two-point functions are consistent with the expectation, however, the errors are too large to allow for quantitatively meaningful statements. For $|\boldsymbol{p}| \approx 1.88$ GeV (Fig. 5), within our statistics of one source position on 200 gauge configurations, it turned out to be impossible to obtain effective energies without momentum smearing at all.

The same comparison is shown for the nucleon in Figs. 6 and 7, where in Fig. 7 we also include a momentum as high as $|\boldsymbol{p}| \approx 2.82$ GeV. In this case we show the lattice dispersion relation Eq. (41) of a free Wilson fermion with

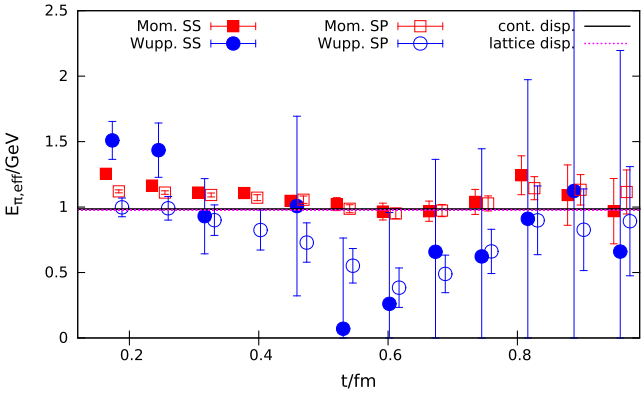

FIG. 4. Effective pion energies Eq. (48) for the lattice momentum $\boldsymbol{P} = (1,1,1)$, corresponding to $|\boldsymbol{p}| \approx 0.94$ GeV. In the case of momentum smearing (squares), we set $\boldsymbol{K} = \zeta \boldsymbol{P}$ with $\zeta = 0.8$. Solid symbols correspond to smeared-smeared, open symbols to smeared-point two-point functions. Some data points are shifted horizontally to enhance the legibility. The expectations from the continuum and lattice dispersion relations can be found in Eqs. (39) and (40), respectively. Symbols are shifted horizontally for better legibility.

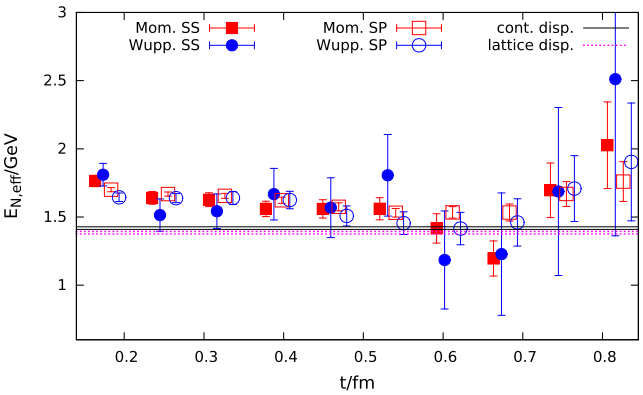

FIG. 6. The same as Fig. 4 for the nucleon and $\zeta = 0.5$. The horizontal lines correspond to the expectations from the continuum and lattice dispersion relations Eqs. (39) and (41), respectively.

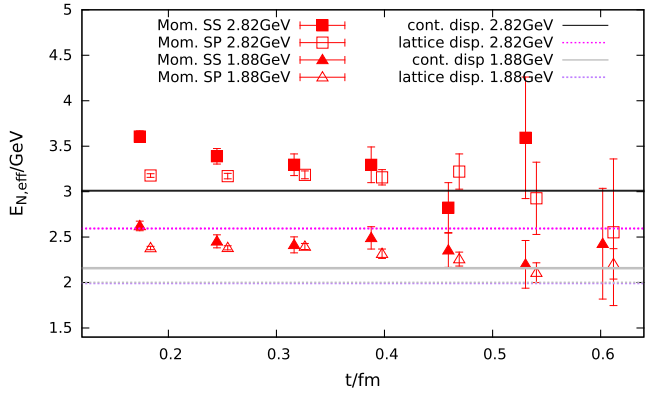

FIG. 7. The same as Fig. 6 for $\boldsymbol{P} = (2,2,2)$ ($\zeta = 0.4$) and $\boldsymbol{P} = (3,3,3)$ ($\zeta = 0.44$), corresponding to $|\boldsymbol{p}| \approx 1.88$ GeV and $|\boldsymbol{p}| \approx 2.82$ GeV, respectively. Again, the conventional Wuppertal smearing data are too noisy to allow for the extraction of effective energies.

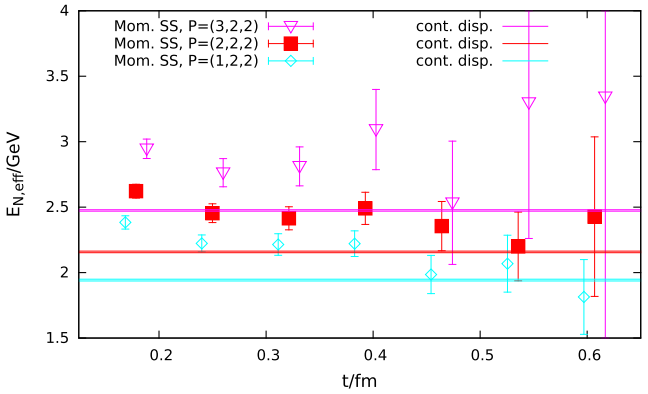

FIG. 8. The nucleon smeared-smeared effective energy with one and the same momentum smearing $\boldsymbol{K} = (0.8, 0.8, 0.8)$, optimized for $\boldsymbol{P} = (2,2,2)$, but for momenta pointing into different directions. Symbols are shifted horizontally for better legibility.

the nucleon mass given in Eq. (38). The statistical errors of the momentum smeared data again are much smaller than for the nonmomentum smeared cases. Like for the pion, it was impossible within our statistics to extract effective energies for momenta larger than 1.5 GeV. At $|\boldsymbol{p}| \approx 0.94$ GeV the data agree with the expectation for $t \gtrsim 0.6$ fm while for the higher momenta, where the statistical errors are larger, the data are consistent with plateaus starting at $t \gtrsim 0.45$ fm. For the high momenta shown in Fig. 7 the data seem to prefer the continuum dispersion relation over the lattice dispersion relation Eq. (41).

It is clear from the results shown above that the gain of using momentum smearing is tremendous. The only drawback, in addition to the computational overhead from the smearing itself, is that each value of the parameter $\boldsymbol{k}$ employed at the source requires us to recompute the respective quark propagator. A natural question therefore is whether it is possible to efficiently realize several momenta $\boldsymbol{p}$ using one and the same smearing vector $\boldsymbol{k}$. We already know from Fig. 3 that for $\boldsymbol{p} \| \boldsymbol{k}$ the proportionality constant ζ defined in Eq. (47) can be varied by about 20% without a significant deterioration and by much more if one is willing to accept a compromise: comparing Fig. 3 with Fig. 4 reveals that even a much less than perfect momentum smearing is a tremendous improvement over the conventional $\zeta = 0$ case. We may also ask whether it is possible to (slightly) vary the direction of $\boldsymbol{p}$ relative to $\boldsymbol{k}$. This of course is potentially dangerous since the interpolator used will not transform anymore according to an irrep of the little group of O_h (or its double cover), associated to the momentum direction. However, if for instance we are only interested in the ground state mass of a spin-0 or spin-1/2 hadron this should not be a major problem. Figure 8 demonstrates that to a certain extent varying the momentum direction for a fixed $\boldsymbol{k}$ appears feasible too. In all the cases shown it is impossible to extract any meaningful effective energies without momentum smearing.

C. Test of boosted (momentum) smearing

It has been suggested by two groups [32,33] that introducing an anisotropy and thereby Lorentz boosting the smearing function may improve the overlap of high momentum interpolators with the respective hadronic ground states. We generalize these ideas to off-axis momentum directions, also incorporating phase factors, in the Appendix, see Eqs. (A6)–(A10). Length contractions depend on the choice of coordinates and in particular on time differences in the moving frame relative to the rest frame. Since in Euclidean spacetime all distances are spacelike and any real time information is lost, it is not clear to us why spatial distances should be subjected to a Lorentz boost. Our numerical observations are negative.

In Fig. 9, which is representative for our experiences, we show effective pion energies for $\boldsymbol{P} = (3,0,0)$, corresponding to $|\boldsymbol{p}| \approx 1.63$ GeV and a boost factor

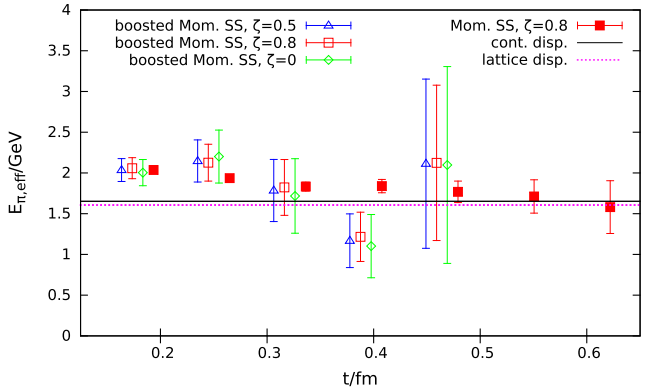

FIG. 9. Effective smeared-smeared pion energies for $\boldsymbol{P} = (3,0,0)$, corresponding to $|\boldsymbol{p}| \approx 1.63$ GeV: momentum smearing with the optimized parameter $\zeta = 0.8$ and boosted momentum smearing Eq. (A6) for $\gamma \approx 5.6$ with $\zeta = 0.5, 0.8, 0$. Symbols are shifted horizontally for better legibility.

$\gamma = E_\pi(p)/m_\pi \approx 5.6$, close to the one that corresponds to the bottom right panel of Fig. 2 ($\gamma = 5.3$). In this case it was again not possible to extract effective energies using the conventional Wuppertal smearing. All Lorentz contracted (boosted) interpolators give results much inferior to the one obtained using the unboosted momentum smearing. This also holds for different contraction factors $1/\gamma$ (not shown). At the same time the boost enhances the signal relative to unboosted Wuppertal smearing, without the momentum phase factor. In the figure we show boosted smearing results for different momentum shifts: $\boldsymbol{k} = \boldsymbol{0}$, the naive expectation $\boldsymbol{k} = 0.5\boldsymbol{p}$ and the case that is close to optimal without the boost applied, $\boldsymbol{k} = 0.8\boldsymbol{p}$. We find the effective energies and their uncertainties are quite insensitive to the $\boldsymbol{k}$ value. This is not surprising since the support of the smearing function in the direction of the momentum is quite small. At the same time this small support may explain why the boost outperforms conventional Wuppertal smearing as broad wave functions are disfavored at high momenta, unless the $\boldsymbol{k}$ vector is introduced, see Eq. (29).

In summary, substantially contracting the smearing function in the direction of the momentum ameliorates the phase mismatch discussed in this article. Therefore, some improvement over the conventional isotropic smearing case can be achieved. However, only momentum smearing correctly accounts for this effect and we see no indication that injecting a momentum alters the optimal shape of the modulus of the smearing function Eq. (45).

D. Comparison with dispersion relations

Our main aim here was to demonstrate the effectiveness of momentum smearing. For this purpose it was sufficient to consider only one source position on 200 individual gauge configurations. The present state-of-the-art, however, is to realize multiple sources on ten times as many configurations. In the near future we will compute a multitude of physically interesting observables with enhanced statistics. The masses shown in Eq. (38) were already obtained with high statistics and in Figs. 3–9 we have compared effective energies against the continuum and lattice dispersion relations Eqs. (39)–(41), using these values.

In all cases the smeared-smeared effective energies from optimized momentum smearing were in agreement with plateaus from $t \geq t_{\min} = 8.5a \approx 0.61$ fm onwards, where $t = 8.5a$ corresponds to the effective energy obtained from the correlation function at $8a$ and $9a$, see Eq. (48). In many cases $t_{\min}$ could be chosen smaller. For the moment being, we conservatively approximate the energies by $E_H(\boldsymbol{p}) \approx E_{H,\mathrm{eff}}(\boldsymbol{p}, t_{\min})$. The results as a function of $\boldsymbol{p}$ are shown in Figs. 10 and 11 and compared to the dispersion relation expectations. We also display results obtained with conventional smearing for small momenta where this is possible. For the two-point functions studied here the precision of the conventional results can be improved at little computational overhead by averaging over (for the absolute momentum values shown) six, eight or twelve equivalent directions. We have not done this, to allow for a "fair" comparison of the efficiency of the smearing methods. It is clear from the figures, however, that the maximally possible error reduction, assuming different momentum direction results to be statistically uncorrelated, would not affect any of our conclusions.

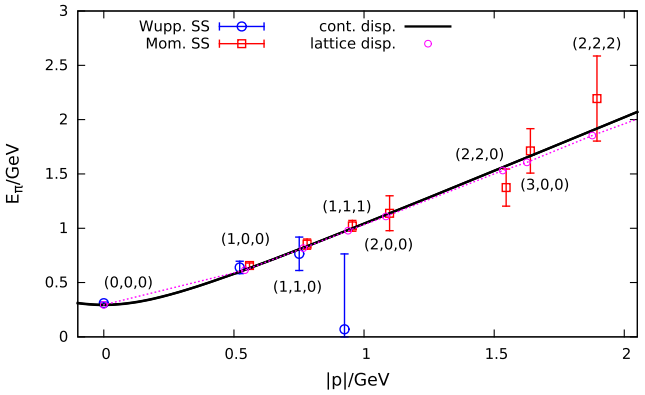

FIG. 10. Pion energies for different lattice momenta. in comparison to the continuum (solid curve) and lattice (points connected by dotted lines) dispersion relations Eqs. (39) and (40).

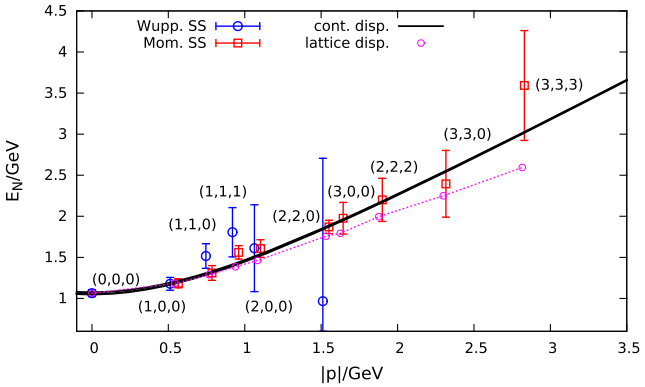

FIG. 11. Nucleon energies for different lattice momenta. in comparison to the continuum (solid curve) and lattice (points connected by dotted lines) dispersion relations Eqs. (39) and (41).

We do not expect either parametrization shown in Figs. 10 and 11 to perfectly describe the data as the lattice dispersion relations are for point particles, assuming a particular form of the effective Lagrangian. However, differences between the two functions are indicative for the size of possible lattice effects. While in the pion case differences between the parametrizations are on the present level of statistics insignificant, the nucleon data appear to be better described by the continuum dispersion relation. In the near future we will further investigate this, increasing our statistics and also employing a different smearing as described in Sec. III E.

VI. CONCLUSION

In many lattice gauge theory applications hadrons carrying high momenta are required. Due to the exponential increase of relative errors of n-point functions with Euclidean time distances and diminishing ground state sampling, high momenta previously were very difficult or impossible to achieve. In Sec. II we have introduced a new class of quark smearing methods for the construction of hadronic interpolators that address and substantially mitigate these problems. One particular realization of these methods, that is trivial to implement and comes with very little computational overhead, is momentum Wuppertal smearing, defined in Eq. (24). We tested this very successfully in Sec. V B, enabling us to determine pion and nucleon energies for momenta as high as almost 2 GeV and 3 GeV, respectively, with just 200 measurements, see Figs. 10 and 11. These figures also include a comparison with the conventional method.

In Sec. V C we investigated the possibility of introducing an (additional) Lorentz boost [32,33]. With and without a momentum phase factor included, this gave some improvement over unboosted Wuppertal smearing, possibly due to a dampening of the phase mismatch by the more rapid falloff of the interpolating wave function in the direction of the momentum. However, the results obtained were inferior to those of momentum Wuppertal smearing, without any boost applied. We conclude that the intuition of contracting the wave function may be unjustified since the hadron is moving in real time but not in imaginary (Euclidean) time.

Iterative methods (momentum smearing or not) suffer from high iteration counts $n \propto a^{-2}$ as the continuum limit $a \to 0$ is approached, in addition to the naive volume factor due to an increasing number of lattice sites. Therefore, in Sec. III E we introduce other noniterative (momentum) smearing methods that may be more suitable for small lattice spacings and that also allow for the construction of non-Gaussian shapes. These will be used by us in the near future.

Realizing momenta that are much larger than the hadron masses of interest is of fundamental importance in several modern applications, e.g., in direct determinations of (quasi) distribution amplitudes [10–12], of (quasi) (generalized) parton distributions [6–9] and moments of transverse momentum distributions [2–5]. The new method allowed us to extract nucleon masses (employing very moderate computational resources) up to momenta $\boldsymbol{p}^2 \approx 7.9\ \mathrm{GeV}^2$. This clearly makes the above observables amenable to lattice simulations in a realistic setting. For three-point functions, these methods potentially even allow for virtualities $Q^2 = 4\boldsymbol{p}^2 \approx 30\ \mathrm{GeV}^2$, switching a source momentum of $-\boldsymbol{p}$ into a sink momentum of $+\boldsymbol{p}$. The computation of these quantities with the new smearing is, depending on the observable, either in progress or planned.

ACKNOWLEDGMENTS

This research was funded by the Deutsche Forschungsgemeinschaft Grant No. SFB/TRR 55. The authors benefited from discussions with Vladimir Braun, Robert Edwards and Jian-Hui Zhang. We also thank Nilmani Mathur, Sasa Prelovsek and Rainer Sommer for comments relating to an earlier version of the manuscript. Gunnar S. Bali acknowledges the hospitality of the Mainz Institute for Theoretical Physics (MITP) where a part of this article was written. We used the CHROMA [51] software package along with the LibHadronAnalysis library and the multigrid solver implementation of Ref. [52] (see also Refs. [53–55]). Computations were performed on Regensburg's QPACE B Xeon Phi system and on the SFB/TRR 55 QPACE 2 [56] Xeon Phi installation in Regensburg. We thank Sara Collins, Peter Georg, Benjamin Gläßle and Daniel Richtmann for their help and technical support.

APPENDIX: BOOSTED (MOMENTUM) SMEARING

We describe how we introduce an anisotropy into (momentum) Wuppertal smearing to introduce a Lorentz contraction of the smearing function [32,33] along the momentum direction proportional to $1/\gamma$, where in the continuum

$$\gamma = E(\boldsymbol{p})/m = \sqrt{1 + \frac{\boldsymbol{p}^2}{m^2}} \geq 1. \tag{A1}$$

Note that m above denotes the hadron mass and the hadron momentum $\boldsymbol{p}$ differs from the momentum smearing parameter $\boldsymbol{k}$. We remark that as we are using equal Euclidean time interpolators there is no compelling reason why such a boost should be applied.

In order to "boost" the smearing function we need to replace

$$\boldsymbol{\nabla} + i\boldsymbol{k} \mapsto \left(\frac{\boldsymbol{\nabla}_\parallel}{\gamma} + \boldsymbol{\nabla}_\perp\right) + i\left(\frac{\boldsymbol{k}_\parallel}{\gamma} + \boldsymbol{k}_\perp\right) \tag{A2}$$

within Eq. (23), where $\boldsymbol{\nabla}_\parallel = \boldsymbol{e}(\boldsymbol{e}\cdot\boldsymbol{\nabla})$, $\boldsymbol{\nabla}_\perp = \boldsymbol{\nabla} - \boldsymbol{\nabla}_\parallel$ and

$$\boldsymbol{e} = \frac{\boldsymbol{p}}{|\boldsymbol{p}|} = \frac{\boldsymbol{k}}{|\boldsymbol{k}|}. \tag{A3}$$

For the Laplacian this means

$$\Delta \mapsto \frac{\boldsymbol{\nabla}_\parallel^2}{\gamma^2} + \boldsymbol{\nabla}_\perp^2 = \left(\frac{1}{\gamma^2} - 1\right)\boldsymbol{\nabla}_\parallel^2 + \Delta, \tag{A4}$$

where

$$\nabla_{\parallel}^2 = \sum_{i,j} e_i e_j \frac{\partial}{\partial x_i}\frac{\partial}{\partial x_j}. \tag{A5}$$

One can easily derive a corresponding iterative smearing: Generalizing Eqs. (9)–(14) and (24), we obtain

$$(\Phi^{\gamma}_{(\boldsymbol{k})} q)_{\boldsymbol{x}} = \frac{1}{N}\Bigg\{ q_{\boldsymbol{x}} + \varepsilon' \Bigg[\sum_{j=\pm 1}^{\pm d} N_{|j|} U_{\boldsymbol{x},j} e^{i\boldsymbol{k}\hat{\boldsymbol{\jmath}}} q_{\boldsymbol{x}+\hat{\boldsymbol{\jmath}}} + \left(1-\frac{1}{\gamma^2}\right) \sum_{i\neq j=1}^{d} \frac{e_i e_j}{2} (U_{\boldsymbol{x},j} U_{\boldsymbol{x}+\hat{\boldsymbol{\jmath}},-i} + U_{\boldsymbol{x},-i} U_{\boldsymbol{x}-\hat{\boldsymbol{\imath}},j}) \times e^{i\boldsymbol{k}\cdot(\hat{\boldsymbol{\jmath}}-\hat{\boldsymbol{\imath}})} q_{\boldsymbol{x}+\hat{\boldsymbol{\jmath}}-\hat{\boldsymbol{\imath}}} \Bigg] \Bigg\}, \tag{A6}$$

where

$$N_j = N_j(\gamma, \boldsymbol{e}) = 1 + \left(\frac{1}{\gamma^2} - 1\right) e_j \sum_{i=1}^{d} e_i. \tag{A7}$$

The (arbitrary) normalization factor

$$N = N(\varepsilon', \gamma) = 1 + 2\varepsilon' \left(d - 1 + \frac{1}{\gamma^2}\right) \tag{A8}$$

follows in the free case and is kept to avoid numerical overflow for high iteration counts. Like Eq. (24) this is most easily implemented, replacing the (APE smeared) links $U_{\boldsymbol{x},j}$ by $U_{\boldsymbol{x},j} e^{i\boldsymbol{k}\hat{\boldsymbol{\jmath}}}$ and then iterating Eq. (A6), using these modified transporters, instead of multiplying in the additional phase factors.

We remark that if the momentum is chosen parallel to a lattice axis, the second sum within Eq. (A6) vanishes. In this case the only differences with respect to the momentum Wuppertal smearing defined in Eq. (24) are that shifts in this direction carry a suppression factor $1/\gamma^2$, the normalization factor N and $\varepsilon' \neq \varepsilon$.

The free field solution for n iterations of Eq. (A6) is a Gaussian with a phase factor $e^{i\boldsymbol{k}\cdot\boldsymbol{x}}$ and variance,

$$\sigma^2 = 2na^2 \frac{\varepsilon'}{N(\varepsilon', \gamma)}, \tag{A9}$$

in the directions perpendicular to the momentum, see Eq. (15). Parallel to the momentum the width is reduced by a factor $1/\gamma$, as it should be. The perpendicular variance above can be kept fixed, equating ε'/N with $\varepsilon/(1+2d\varepsilon)$. The resulting relation between the $\gamma = 1$ smearing parameter ε and the boosted parameter ε' reads:

$$\varepsilon' = \frac{\varepsilon}{1 + 2\varepsilon(1 - 1/\gamma^2)} \leq \varepsilon. \tag{A10}$$

[1] W. Detmold, C. Lehner, and S. Meinel, $\Lambda_b \to p\ell^-\bar{\nu}_\ell$ and $\Lambda_b \to \Lambda_c \ell^-\bar{\nu}_\ell$ form factors from lattice QCD with relativistic heavy quarks, Phys. Rev. D **92**, 034503 (2015).

[2] P. Hägler, B. U. Musch, J. W. Negele, and A. Schäfer, Intrinsic quark transverse momentum in the nucleon from lattice QCD, Europhys. Lett. **88**, 61001 (2009).

[3] B. U. Musch, P. Hägler, J. W. Negele, and A. Schäfer, Exploring quark transverse momentum distributions with lattice QCD, Phys. Rev. D **83**, 094507 (2011).

[4] B. U. Musch, P. Hägler, M. Engelhardt, J. W. Negele, and A. Schäfer, Sivers and Boer-Mulders observables from lattice QCD, Phys. Rev. D **85**, 094510 (2012).

[5] M. Engelhardt, P. Hägler, B. U. Musch, J. W. Negele, and A. Schäfer, Lattice QCD study of the Boer-Mulders effect in a pion, Phys. Rev. D **93**, 054501 (2016).

[6] X. Ji, Parton Physics on a Euclidean Lattice, Phys. Rev. Lett. **110**, 262002 (2013).

[7] X. Ji and J.-H. Zhang, Renormalization of quasiparton distribution, Phys. Rev. D **92**, 034006 (2015).

[8] H.-W. Lin, J.-W. Chen, S. D. Cohen, and X. Ji, Flavor structure of the nucleon sea from lattice QCD, Phys. Rev. D **91**, 054510 (2015).

[9] C. Alexandrou, K. Cichy, V. Drach, E. García-Ramos, K. Hadjiyiannakou, K. Jansen, F. Steffens, and C. Wiese (ETM Collaboration), Lattice calculation of parton distributions, Phys. Rev. D **92**, 014502 (2015).

[10] U. Aglietti, M. Ciuchini, G. Corbo, E. Franco, G. Martinelli, and L. Silvestrini, Model independent determination of the light cone wave functions for exclusive processes, Phys. Lett. B **441**, 371 (1998).

[11] A. Abada, P. Boucaud, G. Herdoiza, J.-P. Leroy, J. Micheli, O. Pène, and J. Rodríguez-Quintero, Preliminaries on a lattice analysis of the pion light cone wave function: A partonic signal?, Phys. Rev. D **64**, 074511 (2001).

[12] V. Braun and D. Müller, Exclusive processes in position space and the pion distribution amplitude, Eur. Phys. J. C **55**, 349 (2008).

[13] M. Falcioni, M. L. Paciello, G. Parisi, and B. Taglienti (APE Collaboration), Again on SU(3) glueball mass, Nucl. Phys. **B251**, 624 (1985).

[14] M. Teper, An improved method for lattice glueball calculations, Phys. Lett. B **183**, 345 (1987).

[15] A. Hasenfratz and F. Knechtli, Flavor symmetry and the static potential with hypercubic blocking, Phys. Rev. D **64**, 034504 (2001).

[16] R. Gupta, A. Patel, C. F. Baillie, G. W. Kilcup, and S. R. Sharpe, Exploring glueball wave functions on the lattice, Phys. Rev. D **43**, 2301 (1991).
[17] S. Güsken, U. Löw, K.-H. Mütter, R. Sommer, A. Patel, and K. Schilling, Nonsinglet axial vector couplings of the baryon octet in lattice QCD, Phys. Lett. B **227**, 266 (1989).
[18] S. Güsken, A study of smearing techniques for hadron correlation functions, Nucl. Phys. B. Proc. Suppl. **17**, 361 (1990).
[19] C. Alexandrou, F. Jegerlehner, S. Güsken, K. Schilling, and R. Sommer, B meson properties from lattice QCD, Phys. Lett. B **256**, 60 (1991).
[20] S. Collins (UKQCD Collaboration), Gauge invariant smearing and the extraction of excited state masses using Wilson fermions at $\beta = 6.2$, Nucl. Phys. B, Proc. Suppl. **30**, 393 (1993).
[21] C. R. Allton *et al.* (UKQCD Collaboration), Gauge invariant smearing and matrix correlators using Wilson fermions at $\beta = 6.2$, Phys. Rev. D **47**, 5128 (1993).
[22] G. S. Bali, H. Neff, T. Düssel, T. Lippert, and K. Schilling (SESAM Collaboration), Observation of string breaking in QCD, Phys. Rev. D **71**, 114513 (2005).
[23] P. Lacock, A. McKerrell, C. Michael, I. M. Stopher, and P. W. Stephenson (UKQCD Collaboration), Efficient hadronic operators in lattice gauge theory, Phys. Rev. D **51**, 6403 (1995).
[24] P. Boyle (UKQCD Collaboration), A novel gauge invariant multistate smearing technique, J. Comput. Phys. **179**, 349 (2002).
[25] G. M. von Hippel, B. Jäger, T. D. Rae, and H. Wittig, The shape of covariantly smeared sources in lattice QCD, J. High Energy Phys. 09 (2013) 014.
[26] P. Bacilieri *et al.* (APE Collaboration), The hadronic mass spectrum in quenched lattice QCD: Results at $\beta = 5.7$ and $\beta = 6.0$, Phys. Lett. B **214**, 115 (1988).
[27] W. Detmold, K. Orginos, and Z. Shi, Lattice QCD at non-zero isospin chemical potential, Phys. Rev. D **86**, 054507 (2012).
[28] C. R. Allton, C. T. Sachrajda, V. Lubicz, L. Maiani, and G. Martinelli, A lattice computation of the decay constant of the B meson, Nucl. Phys. **B349**, 598 (1991).
[29] T. A. DeGrand and R. D. Loft, Wave function tests for lattice QCD spectroscopy, Comput. Phys. Commun. **65**, 84 (1991).
[30] T. A. DeGrand and M. Hecht, Observation of orbitally excited hadrons in simulations of lattice QCD, Phys. Lett. B **275**, 435 (1992).
[31] M. J. Peardon, J. Bulava, J. Foley, C. Morningstar, J. Dudek, R. G. Edwards, B. Joó, H.-W. Lin, D. G. Richards, and K. J. Juge (Hadron Spectrum Collaboration), A novel quark-field creation operator construction for hadronic physics in lattice QCD, Phys. Rev. D **80**, 054506 (2009).
[32] D. S. Roberts, W. Kamleh, D. B. Leinweber, M. S. Mahbub, and B. J. Menadue, Accessing high momentum states in lattice QCD, Phys. Rev. D **86**, 074504 (2012).
[33] M. D. Morte, B. Jäger, T. Rae, and H. Wittig, Improved interpolating fields for hadrons at non-zero momentum, Eur. Phys. J. A **48**, 139 (2012).
[34] M. Hamermesh, *Group Theory and Its Application to Physical Problems* (Addison-Wesley, Reading, MA, 1962).
[35] G. S. Bali, S. Collins, and C. Ehmann, Charmonium spectroscopy and mixing with light quark and open charm states from $n_F = 2$ lattice QCD, Phys. Rev. D **84**, 094506 (2011).
[36] F. X. Lee and D. B. Leinweber, Negative parity baryon spectroscopy, Nucl. Phys. B, Proc. Suppl. **73**, 258 (1999).
[37] M. Göckeler, R. Horsley, H. Oelrich, H. Perlt, D. Petters, P. E. L. Rakow, A. Schäfer, G. Schierholz, and A. Schiller, Nonperturbative renormalization of composite operators in lattice QCD, Nucl. Phys. **B544**, 699 (1999).
[38] Z. S. Brown and K. Orginos, Tetraquark bound states in the heavy-light heavy-light system, Phys. Rev. D **86**, 114506 (2012).
[39] G. S. Bali and G. Endrődi, Hadronic vacuum polarization and muon $g-2$ from magnetic susceptibilities on the lattice, Phys. Rev. D **92**, 054506 (2015).
[40] R. Sommer, Leptonic decays of B and D mesons, Nucl. Phys. B, Proc. Suppl. **42**, 186 (1995).
[41] M. Foster and C. Michael (UKQCD Collaboration), Hadrons with a heavy color adjoint particle, Phys. Rev. D **59**, 094509 (1999).
[42] A. Billoire, E. Marinari, and G. Parisi, Computing the hadronic mass spectrum. Eight is better than one, Phys. Lett. **162B**, 160 (1985).
[43] S. Basak, S. Datta, M. Padmanath, P. Majumdar, and N. Mathur, Charm and strange hadron spectra from overlap fermions on HISQ gauge configurations, *Proc. Sci.*, LATTICE2012 (2012) 141, [arXiv:1211.6277].
[44] P. F. Bedaque, Aharonov-Bohm effect and nucleon nucleon phase shifts on the lattice, Phys. Lett. B **593**, 82 (2004).
[45] C. T. Sachrajda and G. Villadoro, Twisted boundary conditions in lattice simulations, Phys. Lett. B **609**, 73 (2005).
[46] G. S. Bali, S. Collins, B. Gläßle, M. Göckeler, J. Najjar, R. H. Rödl, A. Schäfer, R. W. Schiel, A. Sternbeck, and W. Söldner (RQCD Collaboration), The moment $\langle x \rangle_{u-d}$ of the nucleon from $N_f = 2$ lattice QCD down to nearly physical quark masses, Phys. Rev. D **90**, 074510 (2014).
[47] G. S. Bali, S. Collins, B. Gläßle, M. Göckeler, J. Najjar, R. H. Rödl, A. Schäfer, R. W. Schiel, W. Söldner, and A. Sternbeck (RQCD Collaboration), Nucleon isovector couplings from $N_f = 2$ lattice QCD, Phys. Rev. D **91**, 054501 (2015).
[48] A. X. El-Khadra, A. S. Kronfeld, and P. B. Mackenzie, Massive fermions in lattice gauge theory, Phys. Rev. D **55**, 3933 (1997).
[49] C. Morningstar and M. J. Peardon, Analytic smearing of SU (3) link variables in lattice QCD, Phys. Rev. D **69**, 054501 (2004).
[50] G. Parisi, Recent progresses in gauge theories, World Sci. Lect. Notes Phys. **49**, 349 (1980); AIP Conf. Proc. **68**, 1531 (1980).
[51] R. G. Edwards and B. Joó (SciDAC, LHP Collaboration and UKQCD Collaboration), The Chroma software system for lattice QCD, Nucl. Phys. B, Proc. Suppl. **140**, 832 (2005).

[52] S. Heybrock, M. Rottmann, P. Georg, and T. Wettig, Adaptive algebraic multigrid on SIMD architectures, *Proc. Sci.*, LATTICE2015 (2016) 036, [arXiv:1512.04506].

[53] D. Richtmann, S. Heybrock, and T. Wettig, Multiple right-hand-side setup for the DD-α AMG, *Proc. Sci.*, LATTICE2015 (2016) 035, [arXiv:1601.03184].

[54] S. Heybrock, B. Joó, D. D. Kalamkar, M. Smelyanskiy, K. Vaidyanathan, T. Wettig, and P. Dubey, Lattice QCD with domain decomposition on intel xeon phi Co-Processors, arXiv:1412.2629.

[55] A. Frommer, K. Kahl, S. Krieg, B. Leder, and M. Rottmann, Adaptive aggregation based Domain Decomposition Multigrid for the lattice Wilson Dirac operator, SIAM J. Sci. Comput. **36**, A1581 (2014).

[56] P. Arts *et al.*, QPACE 2 and domain decomposition on the Intel Xeon Phi, *Proc. Sci.*, LATTICE2014 (2015) 021, [arXiv:1502.04025].